

Tidally Triggered Star Formation in Close Pairs of Galaxies: Major and Minor Interactions

Deborah Freedman Woods

*Department of Astronomy, Harvard University
60 Garden St., Cambridge, MA 02138*

dwoods@cfa.harvard.edu

Margaret J. Geller

*Smithsonian Astrophysical Observatory
60 Garden St., Cambridge, MA 02138*

Elizabeth J. Barton

*Department of Physics and Astronomy, University of California Irvine
4154 Frederick Reines Hall, Irvine, CA 92697*

ABSTRACT

We study star formation in a sample of 346 galaxies in 168 pairs and compact groups drawn from the original CfA2 Redshift Survey and from a follow-up search for companions. We construct our sample with attention to including pairs with luminosity contrast $|\Delta m_R| \geq 2$. These 55 galaxies with $|\Delta m_R| \geq 2$ provide a set of nearby representative cases of minor interactions, a central feature of the hierarchical galaxy formation model. Here we report the redshifts and positions of the 346 galaxies in our sample, and of 136 galaxies in apparent pairs that are superpositions. In the pairs sample as a whole, there are strong correlations between the equivalent width of the H α emission line and the projected spatial and the line-of-sight velocity separation of the pair. For pairs of small luminosity contrast, $|\Delta m_R| < 2$, the member galaxies show a correlation between the equivalent width of H α and the projected spatial separation of the pair. However, for pairs with large luminosity contrast, $|\Delta m_R| \geq 2$, we detect no correlation between the equivalent width of H α and the projected spatial separation. The relative luminosity of the companion galaxy is more important in a gravitational tidal interaction than the intrinsic luminosity of the galaxy. Central star formation across the entire pairs sample depends strongly on the luminosity ratio, $|\Delta m_R|$, a reasonable proxy for the mass ratio of the pair; pairs composed of similarly luminous galaxies produce the strongest bursts of star formation. Pairs with $|\Delta m_R| \geq 2$ rarely have $\text{EW}(\text{H}\alpha) \gtrsim 70 \text{ \AA}$.

Subject headings: galaxies: interacting

1. Introduction

Observational studies demonstrate that tidal interactions between galaxies trigger enhanced star formation activity. Larson & Tinsley (1978) first studied the colors of “normal” and “peculiar” galaxies to show a connection between probable interacting pairs of galaxies and bursts of star formation. Numerous additional studies provide evidence of enhanced star formation activity in apparently interacting systems through measurements of H α emission, galaxy colors, infrared emission, and radio continuum emission (e.g. Hummel 1981; Kennicutt & Keel 1984; Madore 1986; Kennicutt et al. 1987; Jones & Stein 1989; Sekiguchi & Wolstencroft 1992; Keel 1993, 1996; Liu & Kennicutt 1995a,b; Donzelli & Pastoriza 1997; Barton et al. 2000, 2003; Lambas et al. 2003; Nikolic et al. 2004; Kauffmann et al. 2004). Measurements of the equivalent width of H α emission (EW(H α)) show that high values of EW(H α) occur preferentially when the projected spatial separation of the pair is small (Barton et al. 2000; Lambas et al. 2003; Nikolic et al. 2004). Struck (2005) gives a thorough review of galaxy collisions, including the role of collisions in galaxy evolution, and the influence of the large scale dynamics on star formation and nuclear activity.

Numerical simulations of major galaxy-galaxy interactions provide a physical basis for understanding the observations: central bursts of star formation result from strong gaseous inflows (Mihos & Hernquist 1996). The gaseous inflows occur because gravitational tidal torques transfer the angular momentum of the gas outward before the final merger. The gravitational tidal torques arise primarily from non-axisymmetric structure induced in the galaxy by its companion (Mihos & Hernquist 1996). The galaxy structure strongly influences the strength and timing of the burst of star formation triggered by the gaseous inflows. Similarly, numerical simulations of minor mergers show that tidal torques from minor companions provoke non-axisymmetric structure in the main disk galaxy (Hernquist & Mihos 1995).

Over the history of the universe, galaxy-galaxy interactions link the process of star formation with the growth of galaxies. According to hierarchical structure formation models, these interactions play a critical role in the formation and evolution of galaxies (Somerville & Primack 1999; Kauffmann et al. 1999a,b; Diaferio et al. 1999). Simulations show that galaxies grow by accreting other galaxies, most often minor companions (see the merger tree in Wechsler et al. 2002). Encounters between galaxies and minor companions should be the most common type of encounter because of the greater fractional abundance of low luminosity galaxies.

The importance of minor interactions in the galaxy formation process underscores the importance of examining the process observationally. However, identifying minor companions observationally is challenging because (1) magnitude limited redshift surveys naturally contain relatively more pairs of similar magnitude, and (2) directed searches for low-luminosity companions around primary galaxies have inherently low success rates because of contamination by the more abundant background galaxies.

To examine the relative effects of major and minor encounters on central star formation, we compile a sample of galaxy pairs spanning a wide range of luminosity ratios. We build on the pairs

sample of Barton et al. (2000, 2003) with targeted observations of systems with apparently large luminosity contrasts. In our final sample of 168 pairs and compact groups, including 139 with relative photometry, 21% of those with photometry have $|\Delta m_R| \geq 2$.

Simulations of galaxy-galaxy interactions suggest that the burst of central star formation begins at pericentric passage and continues for up to several hundred Myr (e.g. Mihos & Hernquist 1994). We expect the central star formation to decrease as the galaxies move farther apart and as the burst ages and the continuum level rises (Barton et al. 2000). We therefore study the relationship between central star formation and the projected spatial separation. We also investigate how the luminosity ratio, as a proxy for the mass ratio, affects this dependence.

In §2 we specify the selection criteria for our sample. §3 contains the observations and data reduction. We characterize various properties of the sample galaxies in §4, including the classification of starbursts and AGN, the relative magnitude distribution, the absolute magnitude distribution, and the distribution of H α equivalent widths. Our results are in §5. Then in §6 we discuss the results, and we conclude in §7.

2. The Pairs Sample

We assemble a sample of galaxy pairs and compact groups with attention to including minor companions and satellite galaxies for a study of tidally triggered star formation. The 168 galaxy pairs and compact groups that comprise our sample derive from the 786 galaxies in pairs and compact groups identified in the CfA2 Redshift Survey (see Geller & Huchra 1989 for a description of the CfA2 Redshift Survey; Barton et al. 2000, 2001 for the CfA2 pairs sample). The primary member of each pair or group is in Zwicky’s Catalogue of Galaxies and Clusters of Galaxies (Zwicky et al. 1961-8) and in the Updated Zwicky Catalogue (UZC, Falco et al. 1999). The apparent magnitude limit of the UZC, and hence for our primary galaxies, is $m_{Zw} < 15.5$. For one part of our sample, hereafter called the “EB” sample, the secondary galaxy similarly has a limiting magnitude $m_{Zw} < 15.5$; the secondary galaxy is also in the UZC. The EB sample includes 47 pairs and compact groups, which are part of the photometric sample described in Barton et al. (2001, 2003).

We augment the EB sample at large magnitude contrast by a directed search for faint companions. The 121 pairs and compact groups identified by our directed search are presented here for the first time. The new sample, referred to as the “DW” sample, includes apparent companions to the $m_{Zw} < 15.5$ UZC galaxies that were identified by visual inspection of the digitized Palomar (POSS) E plates by Peter Spotts. Spotts searched the digitized plates for apparent companions of $m_R \lesssim 16$ within a projected radius of $\sim 50 h^{-1}$ kpc of the Zwicky galaxies with known redshifts. For a typical spiral galaxy with color $B - R = 1.0$, this limit is roughly $m_{Zw} \sim 17$. We measure redshifts to eliminate interlopers and thus to identify pairs with larger magnitude contrast than are typically well-represented in magnitude limited redshift surveys. Magnitude limited surveys rarely

include pairs with large magnitude contrast because such pairs reside in the tail of the relative magnitude distribution, where there are relatively few galaxies. It is therefore necessary to identify faint companions by a directed search in order to acquire a sample of substantial size containing minor interactions.

The pairs that we target here expand the range of luminosity (mass) ratios we can use to explore the physics of tidal interactions. For galaxies with $m_B \leq -22$ we can observe companions with 10% of the luminosity of the primary (similar to the LMC/Milky Way). In the DW+EB sample, 21% of the pairs have magnitude differences $|\Delta m_R| \geq 2$.

The pairs must be coincident both in projected spatial separation and in recessional velocity, and they must inhabit low density regions. We select pairs with a projected spatial separation of $\Delta D \leq 55 h^{-1}$ kpc and a line-of-sight velocity separation of $\Delta V \leq 1000 \text{ km s}^{-1}$. In the case of a compact group, where the number of galaxies is greater than two, each galaxy must meet the maximum separation limits when compared to at least one other galaxy in the group, not necessarily when compared to all of the galaxies in the group, i.e. they satisfy a standard “friends of friends” algorithm (Barton et al. 1996; Huchra & Geller 1982). Finally, we also require that the galaxies have $cz \geq 2300 \text{ km s}^{-1}$ to limit their angular size relative to the size of the spectrograph slit, and to exclude the Virgo cluster. The galaxies in the DW sample all reside in low density regions, where the smoothed galaxy number density contrast $\rho_{2.5} \leq 2.2$. The measurement $\rho_{2.5}$ is a density smoothed over a $2.5 h^{-1}$ Mpc scale and is normalized to the mean survey density¹. Requiring that the galaxies reside in low density regions minimizes influence from the surrounding environment (Barton et al. 2000), and thus suppresses effects of the morphology-density relation (Dressler 1980). The 47 pairs in the EB sample reside in regions with density contrast $\rho_{2.5} \leq 2.7$, slightly higher than the DW sample but still low enough to suppress effects of the morphology-density relation.

The DW sample is intended to augment the EB sample at low luminosity and consequently at large magnitude contrast between pair galaxies. The EB sample has been analyzed separately in previous papers (Barton et al. 2001, 2003). Because the EB sample was originally chosen for emission line rotation curve measurements, it has a slight bias toward including galaxies with $\text{H}\alpha$ emission. Although the EB sample galaxies do not necessarily contain *high* values of $\text{H}\alpha$ emission, galaxies with *no* $\text{H}\alpha$ emission were preferentially excluded from the sample. Further discussion on the distribution of $\text{H}\alpha$ emission in the DW and EB samples can be found in §4.2. The EB sample contains relatively fewer pairs with large luminosity contrast compared to the DW sample because the EB sample galaxies are magnitude limited; the DW sample galaxies result from our directed search for faint companions. It is necessary to analyze the two samples combined to demonstrate

¹The mean survey density used for the normalization of the galaxy number density contrast, $\rho_{2.5}$ is calculated from the CfA2 Redshift Survey galaxy luminosity function, using the parameters $M^* = -18.8$, $\alpha = -1.0$, $\phi^* = 0.04$ (Marzke et al. 1994). Assuming a cut-off magnitude equal to the faintest absolute magnitude found in the CfA2 Pairs sample, $M_{cut} = -17.5$, a representative value of the mean survey density used for the normalization is $n = 0.035 \text{ (Mpc/h)}^{-3}$. The exact value of the mean survey density is calculated locally and depends on the galactic extinction correction. For more details on the galaxy number density contrast, see Grogan & Geller (1998).

trends in the data across the wide range of luminosity contrasts of the systems.

We obtained medium resolution optical spectra for all 346 of the galaxies in the DW+EB samples using the FAST instrument (Fabricant et al. 1998) on the 1.5-meter Tillinghast telescope at the Whipple Observatory on Mount Hopkins, Arizona. The 47 pairs and compact groups in the EB sample have complete absolute photometry in B and R, observed with the 4-shooter instrument at the Whipple Observatory’s 1.2-meter telescope. We also have complete relative photometry in B and R for 92 of the 121 pairs and compact groups in the DW sample (§3.1), similarly observed with the 4-shooter instrument at the Whipple Observatory’s 1.2-meter telescope. The remaining 29 pairs and compact groups contribute only to the spectroscopic analysis.

Spectroscopic confirmation of apparent companions is important because many are not coincident in redshift space. We measured spectra for 254 galaxies during the years 2003-2004 as part of our directed search for faint companions for the DW sample. We found 118 coincident in redshift space: 54% of the apparent pairs are superpositions. The superpositions are defined as pairs that do not meet our selection criteria of projected spatial separation $\Delta D \leq 55h^{-1}$ kpc and line-of-sight velocity separation $\Delta V \leq 1000 \text{ km s}^{-1}$. The limiting magnitude for our search is roughly $m_{Zw} \sim 17$ ($m_R \sim 16$ on the the POSS-E plates). For the EB sample, because the secondary galaxies satisfy the UZC magnitude limit $m_{Zw} < 15.5$, the fraction of superpositions is smaller. Table 1 lists the position, redshift, and EW(H α) of the newly identified galaxy pairs and compact groups from the CfA2 Redshift Survey, as well as for the previously identified EB galaxy pairs and compact groups included in our analysis. The galaxy’s magnitude difference from its nearest neighbor is indicated when available. Table 2 gives the redshift and position of the galaxies that are superpositions.

Fig. 1 shows the redshift distribution for the DW+EB galaxies. Although the analogous redshift distribution for the UZC galaxies (Falco et al. 1999) peaks at $cz \sim 8500 \text{ km s}^{-1}$, our selection of low density regions excludes the Great Wall (Geller & Huchra 1989) that covers the range $cz = 7000 - 10^4 \text{ km s}^{-1}$.

We measure the completeness of the pairs sample by comparing it with the original CfA2 North and CfA2 South Surveys. The range of right ascension and declination for the surveys includes $8^h \leq \alpha \leq 17^h$ and $8.^{\circ}5 \leq \delta \leq 44.^{\circ}5$ (B1950) for the CfA2 North Survey (Geller & Huchra 1989; Huchra et al. 1990, 1995), and includes $20^h \leq \alpha \leq 4^h$ and $-2.^{\circ}5 \leq \delta \leq 48^{\circ}$ for the CfA2 South Survey (Giovanelli & Haynes 1985, 1989, 1993; Giovanelli et al. 1986; Wegner et al. 1993; Vogeley 1993). Barton et al. (2000) estimate that the original CfA2 pair sample of 786 galaxies in pairs and compact groups is 70% complete with respect to the UZC (Falco et al. 1999). The DW+EB sample is complete with respect to the original CfA2 South Survey for the 95 objects in 47 pairs and compact groups in low density contrast regions $\rho_{2.5} \leq 2.2$ in right ascension range $20^h \leq \alpha \leq 4^h$. The properties of the sub-sample of 95 objects are indistinguishable from those of the DW+EB sample as a whole. A Kolmogorov-Smirnov (K-S) test of the distributions of the EW(H α) for the two sub-samples indicates no systematic differences: the probability that they are drawn from the same parent sample is 45%. Similarly, the K-S test reveals no systematic differences

in the distributions of the absolute magnitudes of the galaxies, the relative magnitudes of the pairs, and the spatial separations of the galaxies from their nearest neighbors in the complete sub-sample compared to the entire DW+EB sample. Hence, the DW+EB sample as a whole is a representative subset of the CfA2 South Survey.

3. Observations and Data Reduction

To characterize the relative and intrinsic luminosities and the color profiles of the galaxies, we obtained photometry in Harris R and B filters. We observed 92 of the 121 pairs from the DW sample with the 4-shooter camera mounted on the Fred Lawrence Whipple Observatory's (FLWO's) 1.2-meter telescope at Mount Hopkins, Arizona, in March, June, and October 2003. Four out of 11 nights were photometric, enabling absolute photometry in B and R for 32 galaxy pairs. We have relative photometry in B and R for all 92 pairs. §3.1 discusses the photometric analysis of the DW sample. Barton et al. (2001, 2003) describe the photometric analysis of the EB sample.

To assess the star formation activity of the galaxies, we measured the EW(H α). We used spectra from the FAST spectrograph (Fabricant et al. 1998) mounted on the Whipple Observatory's Tillinghast 1.5-meter telescope at Mount Hopkins, Arizona, during the years 1994-2004. Most of the spectra for the DW sample are analyzed here for the first time; the spectra for the EB sample are included in previous studies (Barton et al. 2000, 2001, 2003). §3.2 describes the analysis of the 249 galaxy spectra in the DW sample.

3.1. Photometric Sample

We observed each galaxy pair in Harris R and B filters for a total of 5 minutes in R and 10 minutes in B; in most cases we took two exposures for each image. Bias frames, dome flats, sky flats, and dark frames comprised our standard calibration data. When photometric conditions prevailed, we observed Landolt standard star fields (Landolt 1992). We used standard imaging data programs from the IRAF *CCDRED* package to reduce the data. To construct the final image for analysis, we first normalized the sky values by adding a constant value to every pixel in one of the images to equalize the modes of the two images. Then we combined the images with the IRAF task *drizzle* from the STSDAS *dither* package (an implementation of the Drizzle algorithm by Fruchter & Hook 2002.) Where necessary, we cleaned additional bad pixels from the summed images.

We measured galaxy magnitudes with the program SExtractor, a source extraction algorithm developed by Bertin & Arnouts (1996). Using detailed surface photometry measurements from the EB sample as a standard, we calibrated the SExtractor input parameters to extract apparent magnitudes of sources in a set of test images that most closely matched the magnitudes determined from detailed surface photometry for the same test images (Barton et al. 2001). For galaxies with apparent magnitudes > 14.2 , there was no significant offset between the magnitudes determined

by SExtractor (m_{SE}) and by detailed surface photometry (m_{sp}); the relative scatter is 0.05 mag. However, for the galaxies with $m_R < 14.2$, the SExtractor magnitudes were offset by 0.2 mag, and the relative scatter was 0.1 mag (see Fig. 2).

SExtractor failed to detect one or more galaxies in 16 of the pairs when using the calibrated set of input parameters. The usual cause of failure was the apparent location of a galaxy near a bright star or in a crowded field. Modifying the SExtractor input parameters that control the background grid size and detection threshold enabled detection, but the magnitudes obtained using the modified input parameters for SExtractor differed significantly more (by 0.3 mag on average) from the “standard” detailed surface photometry magnitudes. Instead, IRAF aperture photometry (IRAF task *polyphot*) produced much more robust results (m_{IRAF}) for these objects that compared well with the detailed surface photometry; the mean offset is 0.07 mag and the scatter is 0.1 mag in a sample of 10 test objects. We extracted aperture photometry for every member in a group in both the B and R images whenever one galaxy in a group required measurement by aperture photometry. This approach ensures that our measurements of relative magnitudes for galaxies within the group are consistent and shared the same systematic offsets.

We determined the uncertainty in our relative photometry for all of our galaxies, including the bright ones, using the detailed surface photometry as a standard. The standard deviation of the difference between the SExtractor photometry and the detailed surface photometry is 0.12 mag, a conservative estimate of our uncertainty. The uncertainty in the IRAF aperture photometry is similar.

3.2. Spectroscopic Sample

We acquired long-slit spectra with the FAST spectrograph on the FLWO 1.5-meter Tillinghast telescope at Mount Hopkins, Arizona. The spectra covered wavelengths between 4000 and 7000 Å with a dispersion of 300 lines mm⁻¹ and a FWHM of 6.2 Å in a 3'' wide slit. The extracted aperture length ranged from 1.7 to 32''. For the galaxy pairs with $2300 < cz < 16500$ km s⁻¹, the aperture covered from 0.42 to 19.5 kpc across the face of the galaxy ($H_0 = 71$ km s⁻¹ Mpc⁻¹), with most of the light coming from the central region of the galaxy. Spectrophotometric standard stars observed each night provided relative flux calibration.

We measured the EW(H α) from the ratio of the line flux to the continuum immediately around it. We used the IRAF task *splot* to measure the equivalent width of H α and of H β , [N II] (6583 Å), and [O III] (5007 Å) for diagnostics (see §4.1). We simultaneously fit for the [N II] lines (6548 and 6583 Å) around H α in case the lines were blended. To account for Balmer absorption around H β , we measured the equivalent width of emission in a narrow region around the emission line, with the continuum level taken at the base of the absorption trough, if an absorption trough was present. In the case of H α , the presence of the nearby [N II] emission lines made it difficult to determine the depth of the Balmer absorption trough. We adopted values for the residual absorption

corrections measured in the Nearby Field Galaxy Survey (Jansen et al. 2001; Kewley et al. 2002), which has similar spectra and EW measurement techniques. The corrections are 1.5 ± 0.5 Å and 1.0 ± 0.5 Å for EW(H α) and EW(H β), respectively. We note that the uncertainty in the Balmer absorption correction is small compared to the total uncertainty in our measured equivalent widths, as described below.

We surmised, based on multiple exposures of the same galaxy, that the dominant source of error in equivalent width comes not from the method of measuring the emission lines and Balmer absorption, but from the repeatability of the slit position for the exposure. Repeated measurements of the EW(H α) from multiple exposures of the faintest galaxies had an average difference of 18% with an rms scatter of 9%, giving similar results for galaxies with EW(H α) ranging from 5-64 Å (mean EW(H α) = 23 Å). We take 18% as a conservative estimate of the uncertainty in the measurement of equivalent widths; spectra with better signal to noise have a slightly smaller uncertainty.

4. Characteristics of Sample

Here we characterize the properties of our pairs sample. In §4.1 we discuss the spectral classification of the objects as starburst galaxies, AGN, or intermediate type. We then can exclude the objects identified as AGN or intermediate classification from the analysis of tidally triggered star formation. We thus obtain a sample of starburst galaxies with spectra dominated by photoionization from hot stars (e.g. Dopita et al. 2000; Kewley et al. 2001), not by shocks (e.g. Dopita & Sutherland 1995) or by non-thermal or power-law continua (e.g. Koski 1978; Alexander et al. 2000), as is the case for AGN. The distribution of the EW(H α) is described in §4.2. In addition to the spectral properties of our galaxies (§4.2), we also consider the photometric characteristics: §4.3 and §4.4 discuss the relative and absolute magnitude distributions, respectively.

4.1. Starbursts and AGN

Using emission line ratios, we classify galaxies as starburst, AGN, or intermediate. We apply the line diagnostics of Kewley et al. (2001), who derive an updated classification using the ratios of two sets of emission lines (based on the method of Baldwin et al. 1981; Veilleux & Osterbrock 1987). Using the ratios of [O III] $\lambda 5007$ / H β and [N II] $\lambda 6584$ / H α , we classify the 125 galaxies in the DW sample with measurable emission in all four lines. We correct the H α and H β lines for Balmer absorption; we do not correct for reddening because these line ratios are nearly independent of reddening. Fig. 3 shows the classifications and the diagnostic line of Kewley et al. We find one AGN above the Kewley et al. diagnostic line, and two more near the line. Additionally, we find three objects with $\log([N II] \lambda 6584 / H\alpha) > 0$ and [O III] $\lambda 5007$ or H β undetectable. We count these three objects as AGN.

Kauffmann et al. (2003) argue that the Kewley et al. classification using $[\text{O III}] \lambda 5007 / \text{H}\beta$ and $[\text{N II}] \lambda 6584 / \text{H}\alpha$ produces a conservative lower limit to the number of AGN in their sample of 55,757 SDSS objects with all four lines detected at $\text{S/N} > 3$. Kauffmann et al. define a demarcation line based on their empirical study of the positions of the SDSS objects along two apparent branches in the $[\text{O III}] \lambda 5007 / \text{H}\beta$ vs. $[\text{N II}] \lambda 6584 / \text{H}\alpha$ diagram. The Kauffmann et al. classification line includes all objects that potentially harbor an AGN, whether or not the AGN dominates the optical spectra. We find 11 more objects above the Kauffmann et al. demarcation line, which we exclude from our sample of interacting galaxies. There are 6 additional objects in our sample that lie along the Kauffmann et al. demarcation line. We include the 6 objects on the Kauffmann line in our study of interacting galaxies because only a very weak AGN could be consistent with the spectra. The AGN and intermediate galaxies, counting even the weakest ones, make up 18% of the objects with all four lines measurable, and 9% of the total DW sample. Additionally, 5 of the objects in the EB sample were classified as potential AGN (see Barton et al. 2000).

Our fraction of AGN is a lower limit because we do not classify the 93 galaxies without measurable emission in one of the lines $\text{H}\alpha$ and $[\text{N II}] \lambda 6584$, and our cut-off for AGN is conservative when only the two lines $\text{H}\alpha$ and $[\text{N II}] \lambda 6584$ and not $\text{H}\beta$ or $[\text{O III}] \lambda 5007$ are measurable. For comparison, in the spectroscopic survey 15R-North, which includes 3149 galaxies and is 90% complete to $R = 15.4$, Carter et al. (2001) find that 17% of their sample have AGN-like emission, and 12% have unclassifiable emission based on the classification method of Veilleux & Osterbrock (1987). In a sample of 4921 galaxies from the SDSS, Miller et al. (2003) find at least $\sim 20\%$ of the galaxies contain an AGN using the line ratio diagnostics of Veilleux & Osterbrock (1987) and Kewley et al. (2001). Using other methods of classification, which include classifying galaxies by the ratio of two of the emission lines and applying statistical models, Miller et al. find that up to a total of $\simeq 40\%$ of the galaxies may contain an AGN. Ho et al. (1997) find a higher fraction, 43% of their 420 emission line galaxies from a sample of 486 galaxies in a nearly complete, magnitude limited survey ($B_T \leq 12.5$ mag), have “active” nuclei (including transition objects), based on a method that parallels Veilleux & Osterbrock (1987). The fraction of active galaxies in our sample is significantly smaller than that in Ho et al. (1997) because the spectrograph slit for Ho et al.’s study is much smaller compared to the projected size of the galaxy, Ho et al. subtract the stellar continuum from the spectra, and their spectra have higher signal-to-noise. However, our fraction of active galaxies is similar to that of Barton et al. (2001), who find 19/150 (13%) of their objects with significant $\text{H}\alpha$, $\text{H}\beta$, $[\text{O III}]$, and $[\text{N II}]$ emission are AGN, according to the Veilleux & Osterbrock (1987) classification method.

4.2. Distribution of Star Formation Rates

The equivalent width of the $\text{H}\alpha$ emission line measures a combination of starburst age and strength. We compare the distribution of the $\text{EW}(\text{H}\alpha)$ in the DW sample to a “field” galaxy sample, 15R-North (Carter et al. 2001). The 15R-North Survey is a complete, uniform, magnitude

limited ($R \leq 15.4$) spectroscopic survey. The galaxies for the 15R-North Survey were selected from the POSS I E plates, and spectra were measured on the FAST instrument using a slit width of $3''$ and a slit length of $3'$. Thus, the methodology of the 15R-North Survey and the DW sample are in excellent agreement: the galaxies are selected from the same set of plates and measured on the same instrument using the same slit width. Fig. 4 shows the distributions of $\text{EW}(\text{H}\alpha)$ in the DW, EB, 15R-North, and UZC samples.

There is an excess of moderate to high $\text{H}\alpha$ emission in the DW sample compared to a selection of all 15R-North galaxies that fall into the same redshift range and apparent magnitude range as our sample ($2300 < cz < 16500 \text{ km s}^{-1}$, and $m_R \lesssim 17$). As shown in Table 4, we measure $\text{EW}(\text{H}\alpha) > 10 \text{ \AA}$, representing at least mild star formation activity, for 59% (137/231) of the galaxies in the DW sample. In the 15R-North galaxies within the selected redshift range and apparent magnitude range, 25% (421/1675) have $\text{EW}(\text{H}\alpha) > 10 \text{ \AA}$. The distribution of $\text{EW}(\text{H}\alpha)$ of our DW sample also shows a significantly larger fraction of galaxies with high equivalent widths than are present in the 15R-North sample. Of the 15R-North galaxies in the same redshift range and apparent magnitude range as our sample, vigorous star formation, e.g. $\text{EW}(\text{H}\alpha) > 70 \text{ \AA}$, is present in 0.2% (3/1675) of the galaxies. In the DW sample, 9% (20/231) of the galaxies have $\text{EW}(\text{H}\alpha) > 70 \text{ \AA}$. The comparison suggests that a selection favoring close pairs biases the $\text{EW}(\text{H}\alpha)$ distribution toward higher values, as expected if there is a physical connection between the interaction and star formation. We note that the 15R-North Survey includes 298 galaxies in pairs and n-tuples that satisfy our selection criteria: projected spatial separation $\Delta D < 50 \text{ } h^{-1} \text{ kpc}$, line-of-sight velocity separation $\Delta V < 1000 \text{ km s}^{-1}$, and inhabit the same range $2300 < cz < 16500 \text{ km s}^{-1}$. Some of the highest values of $\text{EW}(\text{H}\alpha)$ in the 15R-North sample actually occur for galaxies in pairs. If the pair galaxies in the 15-R North sample were excluded, then the difference in the distributions of $\text{EW}(\text{H}\alpha)$ in the 15-R North sample and the DW sample would be even more pronounced. Despite the inclusion of some pairs in the 15-R North sample, we see that the DW sample, which is composed entirely of pairs and n-tuples, preferentially includes high values of $\text{EW}(\text{H}\alpha)$ compared to the “field” galaxy sample 15R-North.

We also note that the DW and EB samples have remarkably similar distributions of $\text{EW}(\text{H}\alpha)$. There is a very slight increase in the fraction of EB galaxies with $\text{EW}(\text{H}\alpha) > 10 \text{ \AA}$ compared to that in the DW sample, possibly the result of the EB galaxies’ bias toward non-zero $\text{H}\alpha$ emission or more likely due to both the primary and the secondary galaxies’ selection in B, whereas the DW primaries are selected in B and the secondaries in R. However, the fraction of galaxies with *moderate to high* values of $\text{H}\alpha$ emission are identical in the DW and EB samples: 23% of the DW and EB galaxies have $\text{EW}(\text{H}\alpha) > 40 \text{ \AA}$, and 9% have $\text{EW}(\text{H}\alpha) > 70 \text{ \AA}$. The moderate to high values of $\text{EW}(\text{H}\alpha)$ define the envelope of any measurable correlation between $\text{EW}(\text{H}\alpha)$ and ΔD or $|\Delta m_R|$ because they represent galaxies with available gas and orbital positions conducive to triggered star formation.

4.3. Relative Magnitude Distribution

The magnitude differences for the galaxy pairs in the combined DW+EB sample cover the range $0 \leq |\Delta m_R| \leq 4.4$; there are 55 galaxies with $|\Delta m_R| \geq 2$. We measured magnitude differences in the R band for 80% (260/323) of the galaxies in our spectroscopic sample with available photometry. We use the R magnitude difference between pair galaxies as a proxy for the galaxy mass ratio. We use the magnitude differences only to separate our sample into two coarse bins, $|\Delta m_R| < 2$ and $|\Delta m_R| \geq 2$. Fig. 6 shows the distribution of magnitude differences for all of the galaxies, excluding AGN or objects of intermediate classification.

Pairs with $|\Delta m_R| \geq 2$ are particularly interesting because (1) minor interactions are more common than major interactions because minor companions are far more common, (2) hierarchical models of galaxy formation show that minor mergers occur frequently in a galaxy’s history, and (3) the impact of minor interactions on star formation is not well understood from either an observational or theoretical perspective. Therefore, studying the effects of minor interactions is crucial to understanding galaxy formation.

4.4. Absolute Magnitude Distribution

We use the UZC catalog magnitudes to estimate the absolute magnitude for all of the galaxies in our sample with photometry; the UZC contains the apparent magnitude, m_{Zw} , of the primary galaxy and its redshift. We determine the apparent and absolute magnitude of the secondary galaxy from its B magnitude relative to the primary. Because all of our absolute magnitudes are based on the UZC catalog magnitudes, all of our galaxies share any systematic offsets present in the UZC.

We compare our absolute B photometry with the results from the UZC. The difference in magnitude, $m_{B,DW} - m_{Zw}$, for the 34 galaxies with $m_{Zw} \geq 15.0$ observed under photometric conditions shows a mean offset of $\langle m_{B,DW} - m_{Zw} \rangle = 0.32$ mag, where m_{Zw} generally overestimates the apparent magnitude of the galaxy. The most likely reason for the offset is the fainter limiting isophote of our measurements. The standard deviation, $\sigma_{m_{B,DW} - m_{Zw}} = 0.43$ mag. Our comparison with the Zwicky photometry is consistent with Bothun & Cornell (1990), who find that m_{Zw} corresponds well to b_{26} with a scatter of 0.31 mag, in their study of 107 cluster spirals, including 66 galaxies with $m_{Zw} > 14.9$. Grogin & Geller (1999) also find a similar scatter, 0.32 mag, between m_{Zw} and their photometric analysis of 230 galaxies with $m_{Zw} \leq 15.5$ and eight galaxies with $15.6 \leq m_{Zw} \leq 15.7$. Additionally, Grogin & Geller find a negligible bias in the absolute Zwicky magnitudes computed from the apparent Zwicky magnitudes and the UZC redshifts, compared to their absolute magnitudes in the range $-20.5 \lesssim M_{Zw} \lesssim -18$. We conclude that the Zwicky catalog provides satisfactory estimates of the calibrated apparent magnitude, and we use them for all of our galaxies where applicable, in order to maintain internal consistency. Fig. 7 shows the distribution of absolute magnitudes for the DW+EB samples.

5. Results

Our goal is to isolate the observable properties of the galaxy or its companion that influence the star formation over the course of the interaction. Numerical simulations of tidally triggered star formation (e.g. Mihos & Hernquist 1994; Mayer et al. 2001) predict a correlation between the star formation rate and the time since pericentric passage, which is related to the spatial separation of the galaxies. Barton et al. (2000) discovered a correlation between $\text{EW}(\text{H}\alpha)$ and the projected spatial separation ΔD , and between $\text{EW}(\text{H}\alpha)$ and the line-of-sight velocity separation ΔV observationally; studies by Lambas et al. (2003) and Nikolic et al. (2004) confirmed the correlation between galaxy emission line properties and ΔD or ΔV . Here, we extend the observations to pairs with a larger range of relative luminosities than previously explored.

We investigate whether the luminosity contrast of the pair is important for determining the effectiveness of the tidal interaction. In their study of pair galaxies in the 2dF Survey, Lambas et al. (2003) find that the star formation activity in pair galaxies in the 2dF Survey depends on the relative luminosity of the pair. In contrast, for SDSS close pairs with $|\Delta m_z| < 2$, Nikolic et al. (2004) determine that the star formation rate shows no dependence on the luminosity or morphological type of the companion galaxy. However, Nikolic et al. suggest that their results can be reconciled with those of Lambas et al. because the distributions of the luminosity contrast of their samples differ.

We use our sample with $|\Delta m_R| \geq 2$ to begin to disentangle the influence of intrinsic galaxy properties from the influence of relative properties of the pair. In order not to confuse intrinsic galaxy properties with effects of the interaction, we separate the sample by intrinsic luminosity and test for evidence of tidally triggered star formation in each sub-sample. Intrinsically low luminosity galaxies tend to have younger stellar populations and contain more gas and less dust than intrinsically luminous galaxies, and hence larger values of $\text{EW}(\text{H}\alpha)$ independent of tidal interaction with another galaxy. These generally lower mass galaxies are also more strongly affected by supernova triggered star formation (Lada et al. 1978; Elmegreen et al. 1995; Boss et al. 2003), which would not correlate with ΔD .

Galaxy morphology may also be a factor in determining the effectiveness of the tidally triggered star formation, but morphological classification is beyond the scope of this paper. We thus note that ellipticals and some early spiral galaxies, which have less gas and dust, would show smaller $\text{EW}(\text{H}\alpha)$ at every ΔD . The inclusion of elliptical galaxies in our sample weakens correlations between $\text{EW}(\text{H}\alpha)$ and ΔD relative to a sample containing exclusively gas-rich late spirals and irregular galaxies. The gas-rich galaxies in our sample should, however, define the envelope of a measurable correlation between $\text{EW}(\text{H}\alpha)$ and ΔD , if such a correlation prevails.

In §5.1, we examine the correlation between $\text{EW}(\text{H}\alpha)$ and ΔD , and between $\text{EW}(\text{H}\alpha)$ and ΔV for the sample as a whole. We consider the star formation activity in sub-samples of intrinsic luminosity in §5.2. In §5.3, we test the correlation between $\text{EW}(\text{H}\alpha)$ and ΔD for sub-samples selected by relative luminosity, paying particular attention to the pairs with $|\Delta m_R| \geq 2$. We

consider also the relationship between $\text{EW}(\text{H}\alpha)$ and Δm_R .

5.1. $\text{EW}(\text{H}\alpha)$ in the Sample as a Whole

Fig. 8 shows $\text{EW}(\text{H}\alpha)$ vs. ΔD for the 323 galaxies in the DW+EB sample, excluding known AGN. Here we include all galaxies with FAST spectra, whether or not 1.2-meter photometry is available. The $\text{EW}(\text{H}\alpha)$ is correlated with ΔD in the sample as a whole. A Spearman rank correlation test of $\text{EW}(\text{H}\alpha)$ and ΔD produces a correlation coefficient, C_{SR} , of -0.14, indicating that $\text{EW}(\text{H}\alpha)$ and ΔD are anti-correlated. The probability of no correlation, P_{SR} , is 9.2×10^{-3} . Almost all of the largest $\text{EW}(\text{H}\alpha)$ occur for galaxies with small projected spatial separation. At projected spatial separations $\gtrsim 20 h^{-1}$ kpc, very few galaxies in the sample show large $\text{EW}(\text{H}\alpha)$.

The $\text{EW}(\text{H}\alpha)$ is also correlated with ΔV (Fig. 9). A Spearman rank correlation test between $\text{EW}(\text{H}\alpha)$ and ΔV for the 323 galaxies in the DW+EB samples produces $C_{SR} = -0.16$, with $P_{SR} = 3.3 \times 10^{-3}$. Galaxies with large $\text{EW}(\text{H}\alpha)$, indicating strong or recent bursts of star formation, have smaller relative velocities. We thus confirm the results of Barton et al. (2000).

5.2. Intrinsic Luminosity and $\text{EW}(\text{H}\alpha)$

We examine the effect of the intrinsic luminosity of the galaxies on the correlation between $\text{EW}(\text{H}\alpha)$ and ΔD . Here we include only the 260 galaxies with FLWO 1.2-meter photometry, all of which have FAST spectra. We divide the galaxies into subsets by absolute magnitude, where the intrinsically luminous galaxies with $M_{Zw} < M_{Zw}^*$ ($M_{Zw}^* = -18.8$, assuming $h = 1$ Marzke et al. 1994) are considered separately from the low luminosity galaxies with $M_{Zw} > M_{Zw}^*$. We limit $|\Delta m_R| < 2$ for both the intrinsically bright and faint subsets to minimize the influence of the luminosity contrast when studying the galaxy properties as a function of intrinsic luminosity.

The set of 203 galaxies with $|\Delta m_R| < 2$ contains 141 galaxies (69%) with $M_{Zw} < M_{Zw}^*$ and 62 galaxies (31%) with $M_{Zw} > M_{Zw}^*$. A K-S test of the distributions of $\text{EW}(\text{H}\alpha)$ in the two groups shows that the distributions are similar: the probability of their deriving from the same parent sample is 31% (see Fig. 10).

Both subsets of galaxies with $M_{Zw} > M_{Zw}^*$ and with $M_{Zw} < M_{Zw}^*$, where $|\Delta m_R| < 2$, demonstrate a probable correlation between $\text{EW}(\text{H}\alpha)$ and ΔD . The more luminous galaxies, $M_{Zw} < M_{Zw}^*$, show a correlation of $C_{SR} = -0.14$ with $P_{SR} = 9.8 \times 10^{-2}$. The low luminosity galaxies, $M_{Zw} > M_{Zw}^*$, show $C_{SR} = -0.32$ with $P_{SR} = 1.2 \times 10^{-2}$. Both subsets show a similar trend in the correlation between $\text{EW}(\text{H}\alpha)$ and ΔD : higher values of $\text{EW}(\text{H}\alpha)$ correlate with small spatial separations (Figs. 11,12). Our results suggest that the intrinsic luminosity of the galaxy plays little role in the effectiveness of the tidally triggered star formation induced by its companion galaxy.

5.3. Relative Magnitude and EW(H α)

Next we examine the effect of the relative magnitude of the pair on the correlation between EW(H α) and ΔD . Figs. 13,14 show EW(H α) vs. ΔD for the 260 galaxies with FLWO 1.2-meter photometry, grouped by magnitude difference between the galaxy and its nearest neighbor. We separate the galaxies into two subsets, according to $|\Delta m_R|$. The 55 individual galaxies with $|\Delta m_R| \geq 2$ include 25 galaxies (45%) with $M_{Zw} < M_{Zw}^*$, and 30 galaxies (55%) with $M_{Zw} > M_{Zw}^*$. (Note that the number of individual galaxies with $|\Delta m_R| \geq 2$ can be odd because our sample includes multiplets, where the number of galaxies in the compact group > 2 . Each galaxy is compared to its nearest neighbor.) All of the 55 galaxies with $|\Delta m_R| \geq 2$, regardless of M_{Zw} , are included in this study of the effect of the relative magnitude of the pair because we showed in §5.2 that intrinsically luminous and low luminosity galaxies exhibit similar trends in the correlation of EW(H α) and ΔD . We choose the boundary of $|\Delta m_R| = 2$ because it corresponds to a mass ratio of ~ 10 and allows us to probe a region not well covered in other studies. This division provides a decent sample size with $|\Delta m_R| \geq 2$. Changing the boundary by ± 0.3 mag does not qualitatively affect the results.

Applying the Spearman rank test, we find a clear correlation between EW(H α) and ΔD for the 203 galaxies with $|\Delta m_R| < 2$, where $C_{SR} = -0.18$ and $P_{SR} = 9.0 \times 10^{-3}$. The Spearman rank test measures no correlation between EW(H α) and ΔD for the 55 galaxies with $|\Delta m_R| \geq 2$. The absence of galaxies with $\text{EW}(\text{H}\alpha) \gtrsim 70 \text{ \AA}$ is evident for the pairs with $|\Delta m_R| \geq 2$ (Fig. 14). We note, however, that a larger sample of $|\Delta m_R| \geq 2$ pairs at separations $\Delta D < 5 \text{ } h^{-1} \text{ kpc}$ would be helpful for verifying this result.

Comparison of the distributions of EW(H α) provides another test of whether the galaxies in pairs with large or small luminosity contrast are similarly affected by tidal interactions. Fig. 15 shows the distributions of EW(H α) for galaxies with $|\Delta m_R| < 2$ and galaxies with $|\Delta m_R| \geq 2$. The K-S probability of the two distributions deriving from the same parent sample is 8.9×10^{-3} . The galaxies are unlikely to be drawn from the same parent sample. This result suggests that luminosity contrast of the pair influences the strength or age of the tidally triggered star formation.

In addition to testing the influence of the relative luminosity, $|\Delta m_R|$, on the correlation between EW(H α) and ΔD , we also test the correlation between EW(H α) and $|\Delta m_R|$ directly. Fig. 16 shows the relationship between EW(H α) and $|\Delta m_R|$. A Spearman rank test of EW(H α) vs. $|\Delta m_R|$ for all 260 galaxies with FLWO 1.2-meter photometry measures $C_{SR} = -0.13$ with $P_{SR} = 3.6 \times 10^{-2}$. The negative correlation coefficient indicates that pairs with similar magnitudes, small $|\Delta m_R|$, have the largest EW(H α). The galaxies in low luminosity contrast systems, regardless of their intrinsic luminosity, are more strongly affected by the tidal interaction.

At $\Delta D < 5 \text{ } h^{-1} \text{ kpc}$, there is an absence of pairs with $|\Delta m_R| \geq 2$ and very few pairs with $|\Delta m_R| < 2$ (see Figs. 13,14). We have an observational bias against identifying very faint companions close to bright galaxies. The faintest galaxies in the DW sample result from our visual identification of companions around UZC galaxies (§2). Furthermore, low luminosity companions may be tidally

disrupted by the primary galaxy before reaching $\Delta D \sim 0$ (Hernquist & Mihos 1995). It is possible that we fail to observe any galaxies with $|\Delta m_R| \geq 2$ and $\Delta D < 5 h^{-1}$ kpc because they have been disrupted. It is also possible that we cannot detect undisrupted faint objects against the brighter primary.

6. Discussion

The subset of 55 galaxies (21%) of our pairs sample with $|\Delta m_R| \geq 2$ provides an opportunity to extend the study of tidally triggered star formation to minor interactions. The normalized star formation rate for our galaxies, measured in terms of $\text{EW}(\text{H}\alpha)$, depends strongly on the relative luminosity of the galaxies for the $|\Delta m_R| \geq 2$ subset. The highest values of $\text{EW}(\text{H}\alpha)$ occur for the galaxies in pairs of similar luminosity, where $|\Delta m_R| \sim 0$ (Fig. 16).

The normalized star formation rate as a function of projected spatial separation for the minor encounters differs from that of the major encounters. The galaxies with $|\Delta m_R| < 2$ show a clear correlation ($P_{SR} = 9.0 \times 10^{-3}$) between $\text{EW}(\text{H}\alpha)$ and the projected spatial separation, ΔD ; the $|\Delta m_R| \geq 2$ galaxies do not. A larger sample is needed to probe the response to tidal interactions for the brighter and the fainter of the $|\Delta m_R| \geq 2$ galaxies separately.

The correlations we find between $\text{EW}(\text{H}\alpha)$ - ΔD and $\text{EW}(\text{H}\alpha)$ - ΔV for our sample as a whole are in good agreement with the results of Barton et al. (2000)¹. A study by Nikolic et al. (2004) likewise shows an increase in the specific star formation rate at small projected separations < 30 kpc, in their sample of 12,492 SDSS galaxies with $M_r < -20.45$. They detect a correlation between specific star formation rate and projected separation out to 300 kpc for late-type galaxies. Nikolic et al. also find that the specific star formation rate decreases for pairs with increasing recessional velocity differences. Similarly, Lambas et al. (2003) find that their 1258 field galaxy pairs from the 2dF Survey with $z \leq 0.1$ exhibit enhanced star formation for $\Delta D < 25 h^{-1}$ kpc and $\Delta V < 100 \text{ km s}^{-1}$. The work of Hernández-Toledo et al. (2005) further supports the correlation between projected separation of pair galaxies and their star formation rates. Hernández-Toledo et al. study the light concentration C , asymmetry A , and clumpiness S of 66 disk galaxies in spiral-spiral pairs (Hernández-Toledo & Puerari 2001; Karachentsev 1972), compared to a set of 113 non-interacting galaxies and 66 ULIRGs (Conselice 2003), which are associated with recent interactions. They conclude that the CAS parameters of the closest pairs are similar to that of the ULIRGs', while the CAS parameters of the widest pairs are more similar to the isolated galaxy sample. By contrast, Donzelli & Pastoriza (1997) do not find a significant correlation between $\text{EW}(\text{H}\alpha + [\text{NII}])$ and the projected distance between pair galaxies in their study of 27 physical pairs. Their small sample size and possible selection effects make it difficult to evaluate their results.

The numerical simulations of Perez et al. (2005) support the connection between enhanced star formation and the proximity of galaxies in pairs. Their simulated catalog includes galaxies in pairs (3-D separation $r < 100 h^{-1}$ kpc) and galaxies without a close companion formed in a Λ CDM

cosmology. They find that galaxies with a companion closer than $30 \pm 10 h^{-1}$ kpc demonstrate an excess of star formation activity compared to galaxies without a close companion. However, not all pair galaxies have enhanced star formation: 40% of the simulated galaxy pairs with a companion closer than $30 h^{-1}$ kpc do not. The availability of gas, the depth of the potential well, and the physical separation may help determine the tidally driven gaseous inflow that triggers the burst (Barnes & Hernquist 1996; Tissera 2000; Perez et al. 2005). Perez et al.’s analysis of the simulated catalog in 2-D projection yields consistent results for enhanced star formation for galaxies with a companion at projected separation $r_p < 25 h^{-1}$ kpc.

We draw similar conclusions on the effects of absolute luminosity on measured star formation rates to those reported by Lambas et al. (2003) in their study of 2dF field galaxy pairs. In our sample, subsets of intrinsically luminous ($M_{Zw} < M_{Zw}^*$) galaxies and low luminosity galaxies ($M_{Zw} > M_{Zw}^*$) show similar correlations between $\text{EW}(\text{H}\alpha)$ and ΔD . Although Lambas et al.’s method for measuring enhanced star formation differs from ours, their study similarly shows that the intrinsic luminosity of the pair galaxy has no effect on the mean star formation excess when compared to isolated galaxies, although they find that low luminosity galaxies have higher absolute mean stellar birthrate b parameters.

We compare the effects of relative luminosity on star formation activity in our sample with the results of other recent studies. Nikolic et al. (2004) find no dependence on the mass (z-band magnitude) or morphological type (concentration index) of the companion galaxy in their sample of SDSS close pairs. Nikolic et al. examine the distributions of specific star formation rates for subsets of relative z-band magnitude, $-2 < \Delta m_z \leq -1$, $-1 < \Delta m_z \leq 0$, and $0 < \Delta m_z < 2$, and find no evidence for a difference in the distributions at the 50% confidence level. If we divide our sample into similar bins by Δm_R , we find that the distributions of $\text{EW}(\text{H}\alpha)$ for galaxies with $-2 < \Delta m_R \leq -1$ and $-1 < \Delta m_R \leq 0$ have a 49% probability of deriving from the same parent sample, and the galaxies with $0 < \Delta m_R \leq 2$ have a 24% probability of deriving from the same parent sample as the $-2 < \Delta m_R \leq 0$ galaxies. These similarities in distributions of $\text{EW}(\text{H}\alpha)$ are consistent with the results of Nikolic et al.

Extending the comparison of distributions of $\text{EW}(\text{H}\alpha)$ for subsets of luminosity contrast beyond those considered by Nikolic et al. reveals a different story. Our sample shows that the distribution of $\text{EW}(\text{H}\alpha)$ for the $|\Delta m_R| \geq 2$ galaxies has only a 0.9% probability of deriving from the same parent sample as the $|\Delta m_R| < 2$ galaxies. Our results suggest that the luminosity ratio (mass ratio) of the pair does influence the effectiveness of the tidally triggered star formation. The effect becomes apparent only when the luminosity contrast is large.

We find that galaxies in major interactions are more likely to show enhanced star formation

¹Our sample derives from the same parent sample as that of Barton et al. (2000). The samples differ in that our sample includes pairs where the primary member is a UZC galaxy and the companion is identified by follow-up observations, while the sample of Barton et al. (2000) includes only pairs where both members are UZC galaxies. See §2 for our sample selection and §4 for the sample characteristics.

activity than galaxies in minor interactions. Lambas et al. (2003) describe the same general trend in their study of 2dF galaxies: they find that galaxy pairs of similar luminosity, defined as $L_1/L_2 < 0.5$ ($\Delta m < 0.75$), reveal enhanced star formation in both members. Their galaxy pairs of dissimilar luminosity, $L_1/L_2 > 0.5$, show less star formation enhancement than pairs of similar luminosity. In our data, Fig. 16 clearly shows a peak in $\text{EW}(\text{H}\alpha)$ around $\Delta m_R = 0$, and decreases for galaxies with larger magnitude differences. A Spearman rank correlation test of $\text{EW}(\text{H}\alpha)$ and $|\Delta m_R|$ shows that high values of $\text{EW}(\text{H}\alpha)$ correlate with small magnitude differences (i.e. nearly equal luminosities).

In a related field, Dasyra et al. (2005) study the context for ULIRG activity in galaxy merger remnants. Their analysis includes 23 ULIRGs in binary merger remnants that still have two distinct nuclei. Most of the ULIRGs in their sample are triggered by interactions between galaxies of nearly equal mass. The average mass ratio of the pair is 1.5 to 1. Although some of their pairs have a mass ratio of 3 to 1, Dasyra et al. find that galaxy pairs with larger ratios do not produce ULIRGs. Because ULIRGs occur when gas-rich, disk galaxies merge (e.g. Downes & Solomon 1998; Bryant & Scoville 1999), we compare the properties of the ULIRG host galaxies with our interacting pairs. Our results are consistent in that pairs with small magnitude differences (i.e. similar mass) appear to trigger central star formation more effectively than pairs of large magnitude differences.

7. Conclusions

We assemble a sample of 346 galaxies in 168 pairs and compact groups to measure the star formation activity as a function of intrinsic and relative properties of the galaxies. Our sample derives from the CfA2 Redshift Survey pairs sample (see Geller & Huchra 1989 for a description of the CfA2 Redshift Survey; Barton et al. 2000, 2001 for the CfA2 pairs sample). We construct our sample with the aim of including pairs of dissimilar luminosity because minor interactions are important for galaxy formation in the hierarchical formation model (Somerville & Primack 1999; Kauffmann et al. 1999a,b; Diaferio et al. 1999). Our sample contains 21% of the pairs with photometry with $|\Delta m_R| \geq 2$.

To isolate the intrinsic galaxy properties from the properties of the interaction that influence the effectiveness of the tidally triggered star formation, we examine the $\text{EW}(\text{H}\alpha)$ - ΔD correlation and the distributions of $\text{EW}(\text{H}\alpha)$ for various subsets of our sample. We find:

1. Galaxies with $M_{Zw} < M_{Zw}^*$, and galaxies with $M_{Zw} > M_{Zw}^*$ show a correlation between $\text{EW}(\text{H}\alpha)$ and ΔD , provided $|\Delta m_R| < 2$.
2. The distribution of $\text{EW}(\text{H}\alpha)$ for the $M_{Zw} > M_{Zw}^*$ galaxies is similar to the distribution of $\text{EW}(\text{H}\alpha)$ for the $M_{Zw} < M_{Zw}^*$ galaxies, again provided $|\Delta m_R| < 2$.
3. Galaxies in pairs of small luminosity contrast, $|\Delta m_R| < 2$, show a strong correlation between $\text{EW}(\text{H}\alpha)$ and ΔD .

4. Galaxies in pairs of large luminosity contrast, $|\Delta m_R| \geq 2$, show no significant correlation between $\text{EW}(\text{H}\alpha)$ and ΔD .
5. The distribution of $\text{EW}(\text{H}\alpha)$ for the $|\Delta m_R| < 2$ galaxies differs significantly from the distribution of $\text{EW}(\text{H}\alpha)$ for the $|\Delta m_R| \geq 2$ galaxies. Very few galaxies with $|\Delta m_R| \geq 2$ have $\text{EW}(\text{H}\alpha) > 70 \text{ \AA}$, in contrast to the $|\Delta m_R| < 2$ galaxies.
6. The largest values of $\text{EW}(\text{H}\alpha)$ are associated with galaxies in pairs of $|\Delta m_R| \sim 0$.

The relative luminosity (and thus presumably mass) of the companion galaxy is more important in a gravitational tidal interaction than the intrinsic luminosity of the galaxy. Galaxies in pairs of similar luminosity are more strongly affected by tidally triggered star formation than galaxies in pairs with $|\Delta m_R| \geq 2$.

Not all galaxies in the pairs sample exhibit significant star formation: 32% (74/231) of the DW sample has $\text{EW}(\text{H}\alpha) < 3.5 \text{ \AA}$ (corrected for Balmer absorption). Some galaxies fail to respond to gravitational tidal forces because they lack available gas (e.g. Barnes & Hernquist 1996), and other pairs are merely superpositions. The pair galaxies may just be starting to approach each other for the first time and have not yet experienced a close pass in their orbits. Galaxy structure and orbital geometry influence the effectiveness of the tidally triggered star formation (Mihos & Hernquist 1996). Additionally, the lowest mass galaxies could be strongly affected by other energetic processes such as supernova triggered star formation (Lada et al. 1978; Elmegreen et al. 1995; Boss et al. 2003) and could show enhanced star formation activity independent of pair separation.

Our observed correlation between $\text{EW}(\text{H}\alpha)$ and ΔD is consistent with the theoretical interpretation that tidally triggered star formation results from gas driven to the center of the galaxy by tidal interactions just after perigalacticon, disrupting the system and causing a burst of star formation (Mihos & Hernquist 1996). The absence of $|\Delta m_R| \geq 2$ galaxies with values of $\text{EW}(\text{H}\alpha) \gtrsim 70 \text{ \AA}$ suggests that the relative mass of the galaxies influences the effectiveness of tidally triggered star formation. A stronger test of triggered star formation in minor interactions would include more $|\Delta m_R| \geq 2$ pairs at physical separation $\Delta D < 5 h^{-1} \text{ kpc}$, which are an observational challenge.

We thank Daniel Fabricant, Warren Brown, and Lisa Kewley for their insights and assistance throughout this project. We thank Perry Berlind and Mike Calkins for taking the FAST spectra, and we thank Susan Tokarz for her work in reducing the spectra. We also enjoyed numerous conversations with Jenny Greene, Scott Kenyon, and Michael Kurtz. We thank the referee for helpful comments that strengthened the paper and prompted the comparison with the 15R-North Survey. This project was supported in part by the Smithsonian Institution, Harvard University, and the University of California, Irvine.

REFERENCES

Alexander, T., Lutz, D., Sturm, E., Genzel, R., Sternberg, A., & Netzer, H. 2000, *ApJ*, 536, 710

Baldwin, J., Phillips, M. & Terlevich, R. 1981, *PASP*, 93, 5

Barnes, J. E. & Hernquist, L. 1996, *ApJ*, 471, 115

Barton, E., Geller, M., Ramella, M., Marzke, R. O., da Costa, L. N. 1996, *AJ*, 112, 871

Barton, E. J., Geller, M.J., & Kenyon, S.J. 2000, *ApJ*, 530, 660 (BGK)

Barton, E. J., Geller, M. J., Bromley, B. C., van Zee, L., Kenyon, S. J. 2001, *AJ*, 121, 625

Barton Gillespie, E., Geller, M. J. & Kenyon, S.J. 2003, *ApJ*, 582, 668

Bertin, E. & Arnouts, S. 1996, *A&AS*, 117, 393

Boss, A. P. 2003, in Galactic Star Formation Across the Stellar Mass Spectrum, Proc. International Astronomical Observatories in Chile workshop, held 11-15 March 2002 at La Serena, Chile. ed. J. M. De Buizer, & N. S. van der Blieck (San Francisco: Astronomical Society of the Pacific), *ASP Conf. Ser.*, 287, 281

Bothun, G. D., & Cornell, M. E. 1990, *AJ*, 99, 1004

Bryant, P. M. & Scoville, N. Z. 1999, *AJ*, 117, 2632

Carter, B. J., Fabricant, D. G., Geller, M. J., Kurtz, M. J., & McLean, B. 2001, *ApJ*, 559, 606

Conselice, C. J. 2003, *ApJS*, 147, 1

Dasyra, K. M., Tacconi, L. J., Davies, R. I., Genzel, D. L., Naab, T., Burkert, A., Veilleux, S., & Sanders, D. B. 2005, *ApJ*, in press

Diaferio, A., Kauffmann, G., Colberg, J. M., & White, S. D. M. 1999, *MNRAS*, 307, 537

Donzelli, C. J. & Pastoriza M. G. 1997, *ApJS*, 111, 181

Dopita, M. A. & Sutherland, R. 1995, *ApJ*, 455, 468

Dopita, M. A., Kewley, L. J., Heisler, C. A., & Sutherland, R. S. 2000, *ApJ*, 542, 224

Downes, D. & Solomon, P. M. 1998, *ApJ*, 507, 615

Dressler, A. 1980, *ApJ*, 236, 351

Elmegreen, B. G., Kimura, T., & Tosa, M. 1995, *ApJ*, 451, 675

Fabricant, D., Cheimets, P., Caldwell, N., Geary, J. 1998, *PASP*, 110, 79

Falco, E. E. et al. 1999 PASP, 111, 438

Fruchter, A.S. & Hook, R. N. 2002, PASP, 114, 792, 144

Geller, M. J. & Huchra, J. P. 1989, Science, 246, 897

Giovanelli, R. & Haynes, M. P. 1985, AJ, 90, 2445

Giovanelli, R. & Haynes, M. P. 1989, AJ, 97, 633

Giovanelli, R. & Haynes, M. P. 1993, AJ, 105, 1271

Giovanelli, R., Meyers, S. T., Roth, J. & Haynes, M. P. 1986, AJ, 92, 250

Grogin, N. A. & Geller, M. J. 1998, ApJ, 505, 506

Grogin, N. A. & Geller, M. J. 1999, AJ, 118, 2561

Hernández-Toledo, H. M., Avila-Reese, V., Conselice, C. J. Puerari, I. 2005, ApJ, 129, 682

Hernández-Toledo, H. M., & Puerari, I. 2001, A&A, 379, 54

Hernquist, L. & Mihos, J. C. 1995, ApJ, 448, 41

Ho, L. C., Filippenko, A. V., & Sargent, W. L. W. 1997, ApJ, 487, 568

Huchra, J. P., Geller, M. J., & Corwin, H. G., Jr. 1995, ApJS, 99, 391

Huchra, J. P., Geller, M. J., de Lapparent, V., & Corwin, H. G., Jr. 1990, ApJS, 72, 433

Huchra, J. P. & Geller, M. 1982, ApJ, 257, 423

Hummel, E. 1981, A&A, 96, 111

Jansen, R. A., Franx, M. & Fabricant, D. 2001, ApJ, 551, 826

Jones, B. & Stein, W. A. 1989, AJ, 98, 1557

Karachentsev, I. 1972, Comm. Spec. Astrophys. Obs. USSR, 7, 1

Kauffmann, G., Colberg, J. M., Diaferio, A. & White, S. D. M. 1999a, MNRAS, 303, 188

— 1999b, MNRAS, 307, 529

Kauffmann, G. et al. 2003, MNRAS, 346, 1055

Kauffmann, G., White, S. G., Heckman, T. M., Me'nard, B., Brinchmann, J., Charlot, S. Tremonti, C., Brinkmann, J. 2004, MNRAS, 353, 713

Keel, W. C. 1993, AJ, 106, 1771

Keel, W. C. 1996, APJS, 106, 27

Kennicutt, R. C. & Keel, W. C. 1984, APJ, 279, L5

Kennicutt, R. C., Jr., Tamblyn, P., & Congdon, C. W. 1994, ApJ, 435, 22

Kennicutt, R. C., Jr., Keel, W. C., van der Hulst, J. M., Hummel, E., & Roettiger, K. A. 1987, AJ 95, 5

Kewley, L. J., Geller, M. J., Jansen, R. A. & Dopita, M. A. 2002, AJ, 124, 3135

Kewley, L. J., Heisler, C. A., Dopita, M. A., & Lumsden, S. 2001, ApJS, 132, 37

Koo, D. C., Bershady, M. A., Wirth, G. D., Stanford, S. A. & Majewski, S. R. 1994, ApJ, 427, L9

Koski, A. T. 1978, ApJ, 223, 56

Kurtz, M. J. & Mink, D. J. 1998, PASP, 110, 934

Lada, C. J., Elmegreen, B. G., & Blitz, L. 1978, in Protostars and planets: Studies of star formation and of the origin of the solar system (Tucson, Ariz: University of Arizona Press), 341

Lambas, D. G., Tissera, P. B., Alonso, M. S., & Coldwell, G. 2003, MNRAS, 346, 1189

Landolt, A. U. 1992, AJ, 104, 340

Larson, R. B. & Tinsley, B. M. 1978, ApJ, 219, 46

Liu, C. T. & Kennicutt, R. C., Jr. 1995a, ApJ, 450, 547

Liu, C. T. & Kennicutt, R. C., Jr. 1995b, ApJS, 100, 325

Madore, B. F. 1986, in Spectral Evolution of Galaxies, eds. C. Chiosi & A. Renzini (Reidel, Dordrecht), p. 97

Markze, R. O., Huchra, J. P., & Geller, M. J. 1994, ApJ, 428, 43

Mayer, L., Governato, F., Colpi, M. Moore, B., Quinn, T. R., & Baugh, C. M. 2001, Astrophysics and Space Science, 276, 2/4, 375

Mihos, J. C. & Hernquist, L. 1996, ApJ, 464, 641

Mihos, J. C. & Hernquist, L. 1994, ApJL, 425, 1, L13

Miller, C. J., Nichol, R. C., Gómez, P. L., Hopkins, A. M., & Bernardi, M. 2003, ApJ, 597, 142

Nikolic, B., Cullen, H. & Alexander, P. 2004, MNRAS, 355, 874

Perez, M. J., Tissera, P. B., Lambas, D. G. & Scannapieco, C. 2005, A&A, in press

Sekiguchi, K. & Wolstencroft, R. D. 1992, 255, 581

Somerville, R. S. & Primack, J. R. 1999, MNRAS, 255, 581

Struck, C. 2005, Astrophysics Update Vol. 2, in press

Tissera, P. B. 2000, ApJ, 534, 636

Tonry, J. L., & Davis, M. 1979, AJ, 43, 393

Veilleux, S. & Osterbrock, D. E. 1987, ApJS, 63, 295

Vogeley, M. S. 1993, Ph.D. thesis, Harvard Univ.

Wechsler, R. H., Bullock, J. S., Primack, J. R., Kravtsov, A. V., Dekel, A. 2002, ApJ, 568, 52

Wegner, G., Haynes, M. P., & Giovanelli, R. 1993, AJ, 105, 1251

Weinberg, M. D. 2000, ApJ, 532, 922

Zwicky, F., Herzog, E., Wild, P., Karpowicz, M., & Kowal, C. T. 1961-8, Catalogue of Galaxies and Clusters of Galaxies (Pasadena: California Institute of Technology)

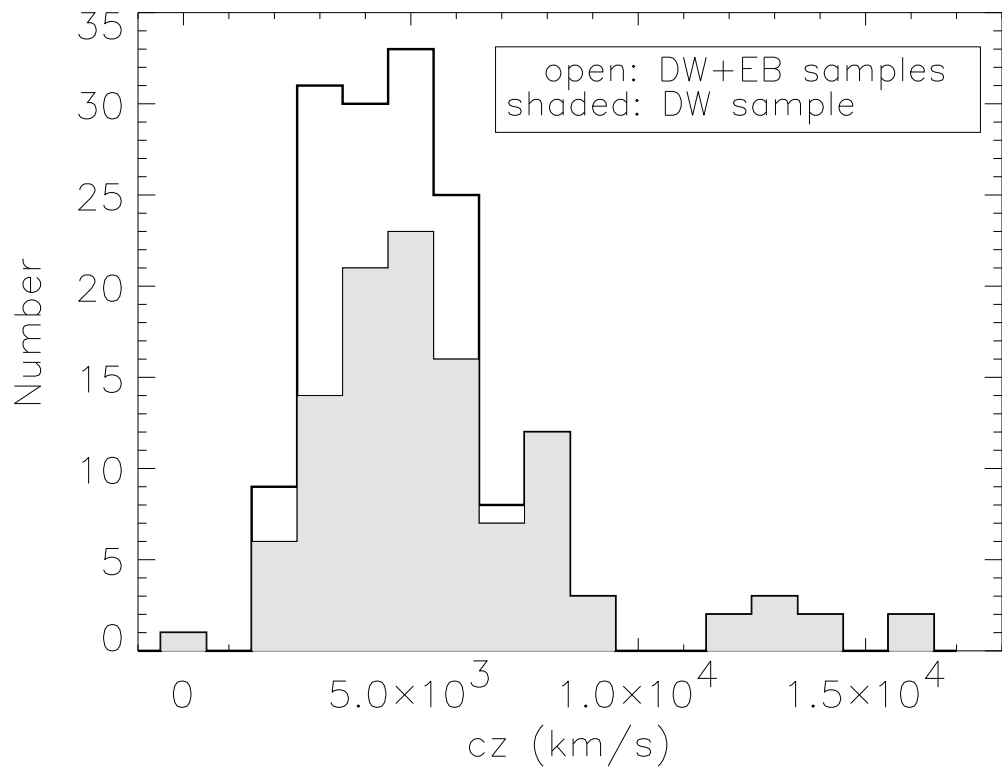


Fig. 1.— The distribution of cz , the average recessional velocity of the pair.

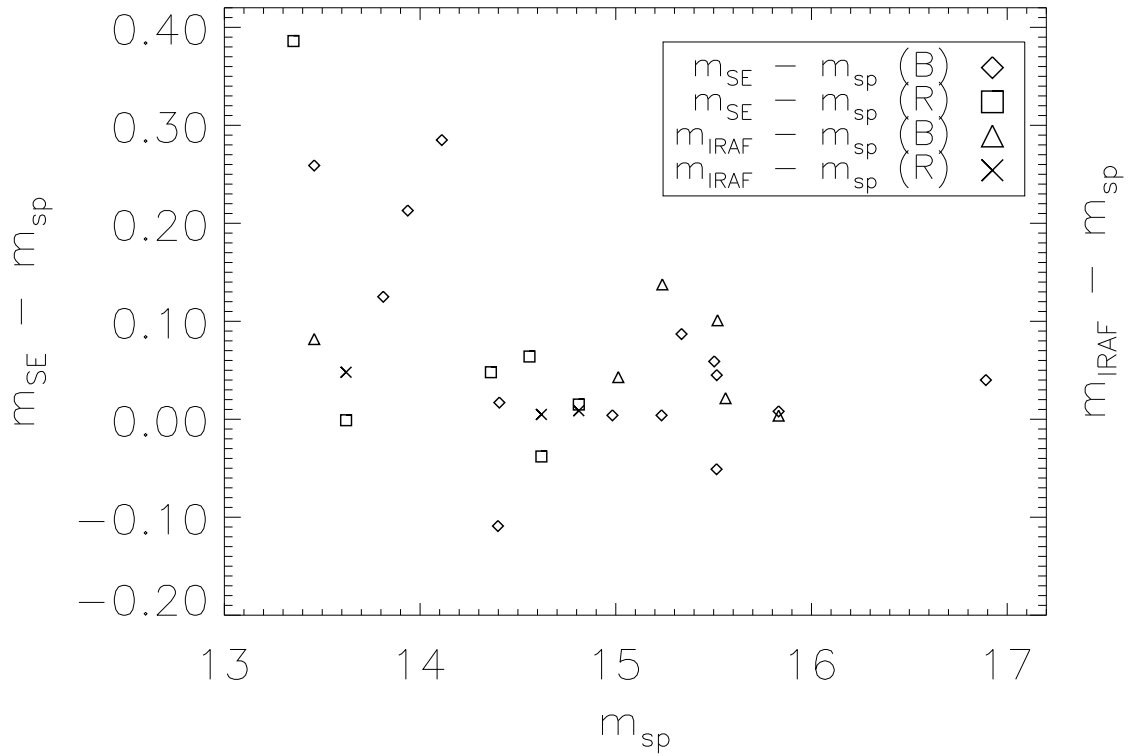


Fig. 2.— Comparisons of $m_{SE} - m_{sp}$ and of $m_{IRAF} - m_{sp}$ measured in the same test images. m_{SE} is the apparent magnitude measured by SExtractor, a source extraction algorithm (Bertin & Arnouts 1996); m_{IRAF} is the aperture magnitude measured with IRAF; and m_{sp} is the apparent magnitude measured by detailed surface photometry (Barton et al. 2001, Barton, private communication, 2003), which we take as our reference.

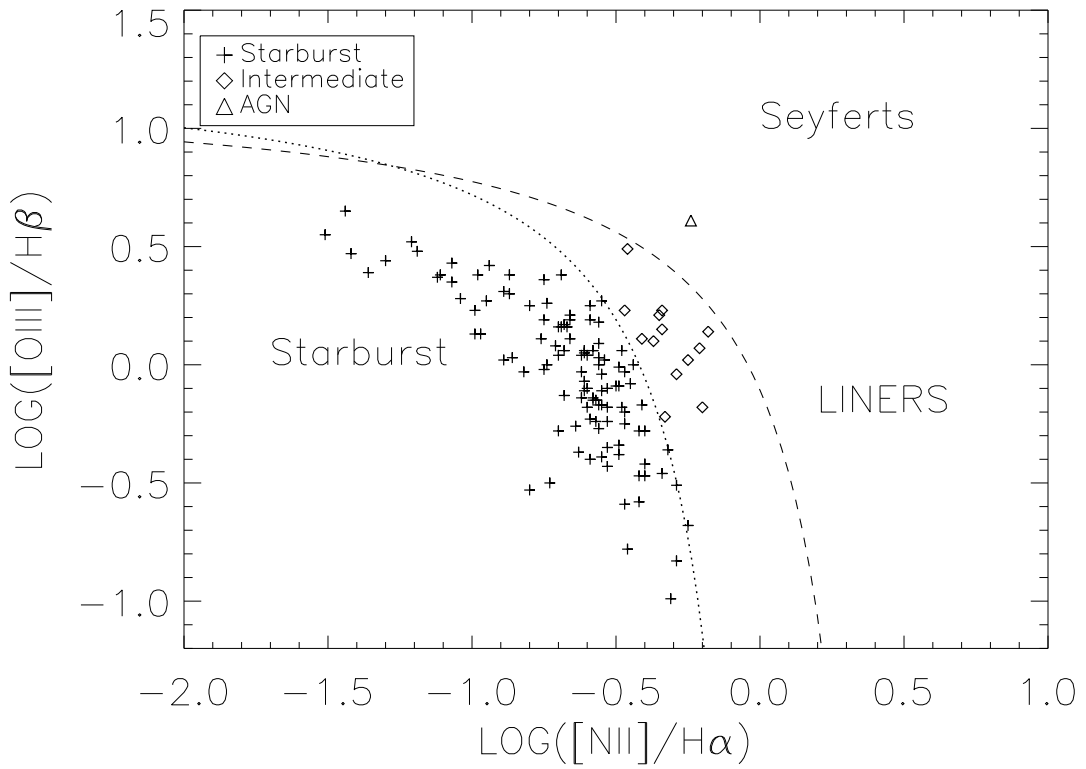


Fig. 3.— Diagnostic diagram showing the identification of starburst galaxies and AGN. The dashed line represents the ionization models of Kewley et al. (2001), and the dotted line represents the empirical studies of Kauffmann et al. (2003).

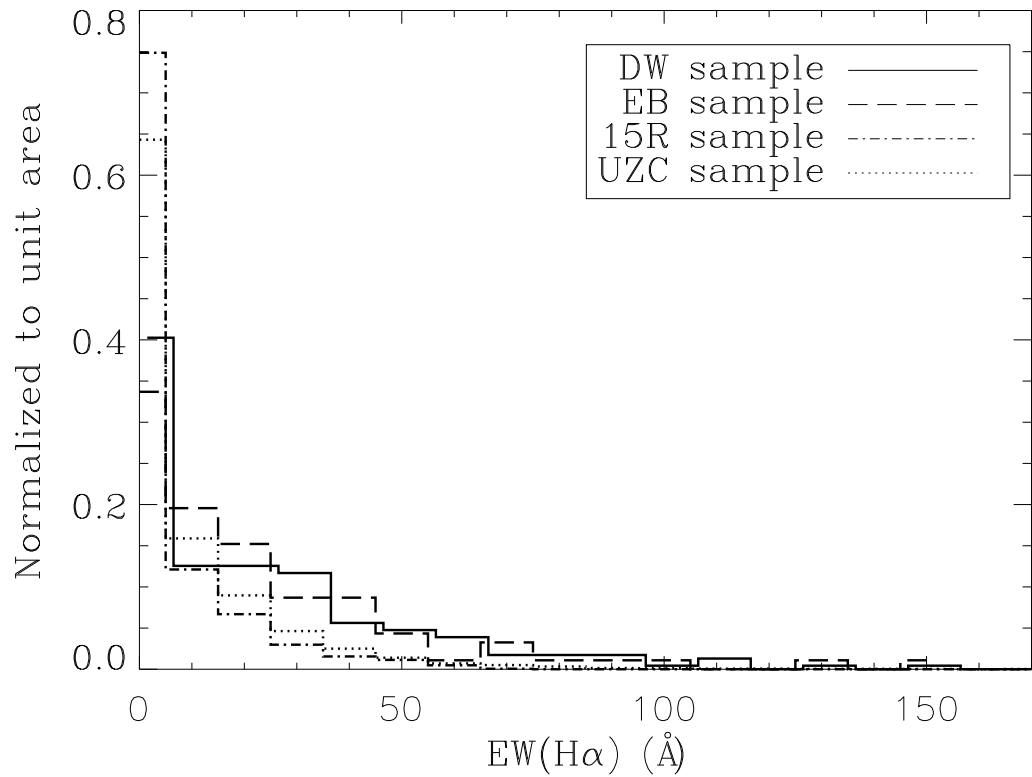


Fig. 4.— Distributions of $\text{EW}(\text{H}\alpha)$ in the DW, EB, 15R-North, and UZC samples in the range 0 to 170 Å. The distributions are normalized to unit area. Galaxies with $\text{EW}(\text{H}\alpha) > 170$ Å are excluded from the figure for the sake of clarity. There are 2 galaxies in the DW sample (0.9%), 2 galaxies in the 15R-North sample (0.1%), and 20 galaxies in the UZC sample (0.2%) with $\text{EW}(\text{H}\alpha) > 170$ Å.

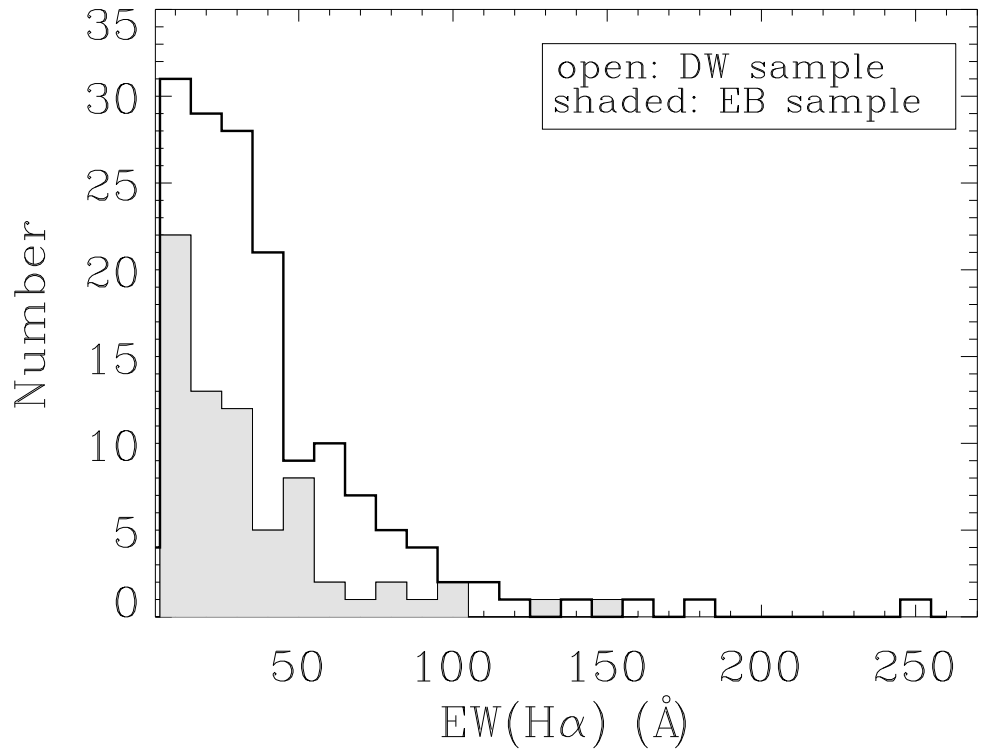


Fig. 5.— Distributions of EW(H α) in the DW and EB samples for the galaxies with $\text{EW}(\text{H}\alpha) \geq 3.5 \text{ \AA}$ (after correction for Balmer absorption). Not shown are the $\text{EW}(\text{H}\alpha) < 3.5 \text{ \AA}$ galaxies, which make up 32% (74/231) of the DW sample and 24% (22/92) of the EB sample.

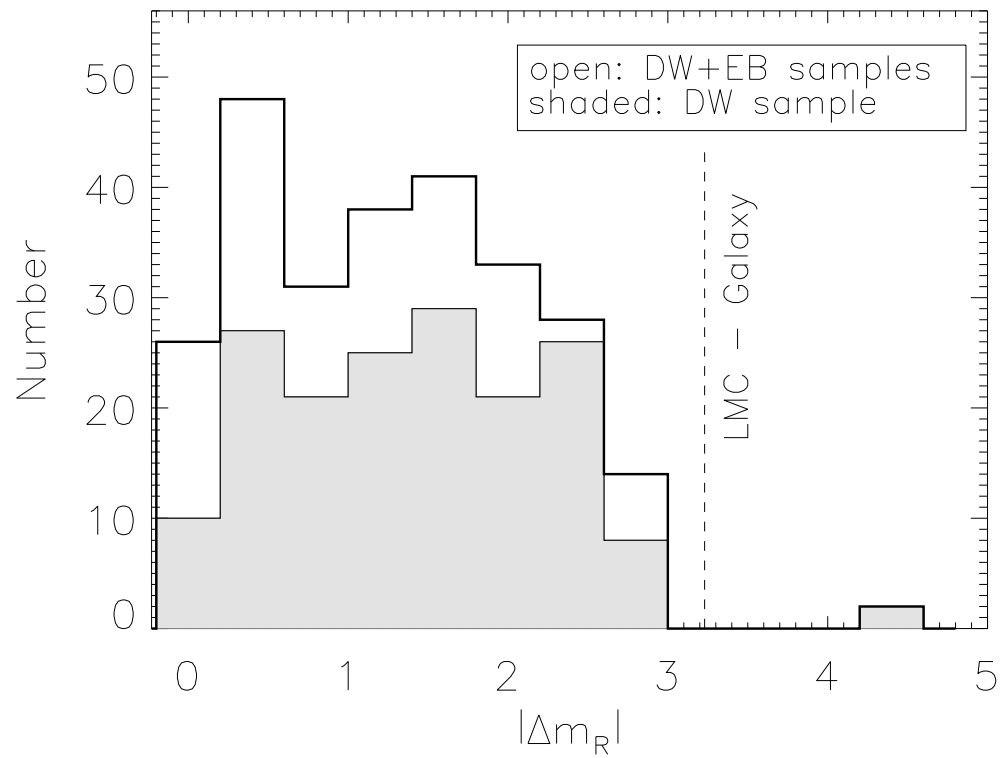


Fig. 6.— Distribution of $|\Delta m_R|$ for the galaxy sample. The uncertainty in $|\Delta m_R|$ is ± 0.17 mag. The dashed line indicates $|\Delta m_R|$ between our Galaxy and the LMC (Weinberg 2000).

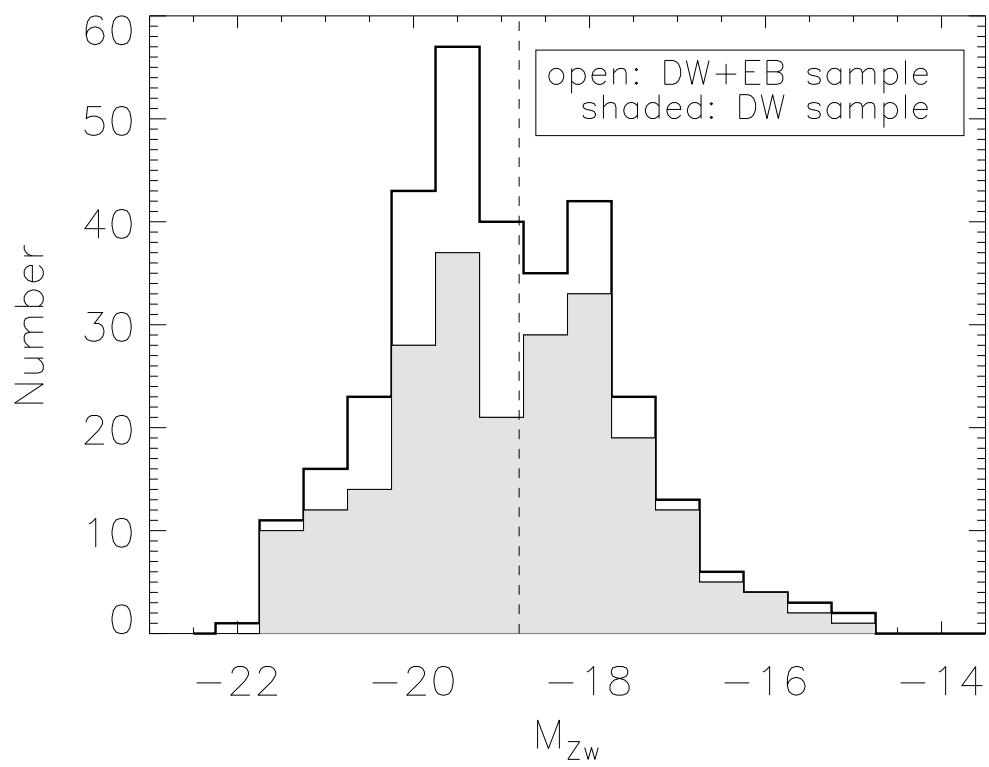


Fig. 7.— Distribution of M_{Zw} in the DW+EB sample. The dashed line shows the value of $M_{Zw}^* = -18.8$ (Marzke et al. 1994) for the CfA2 Redshift Survey.

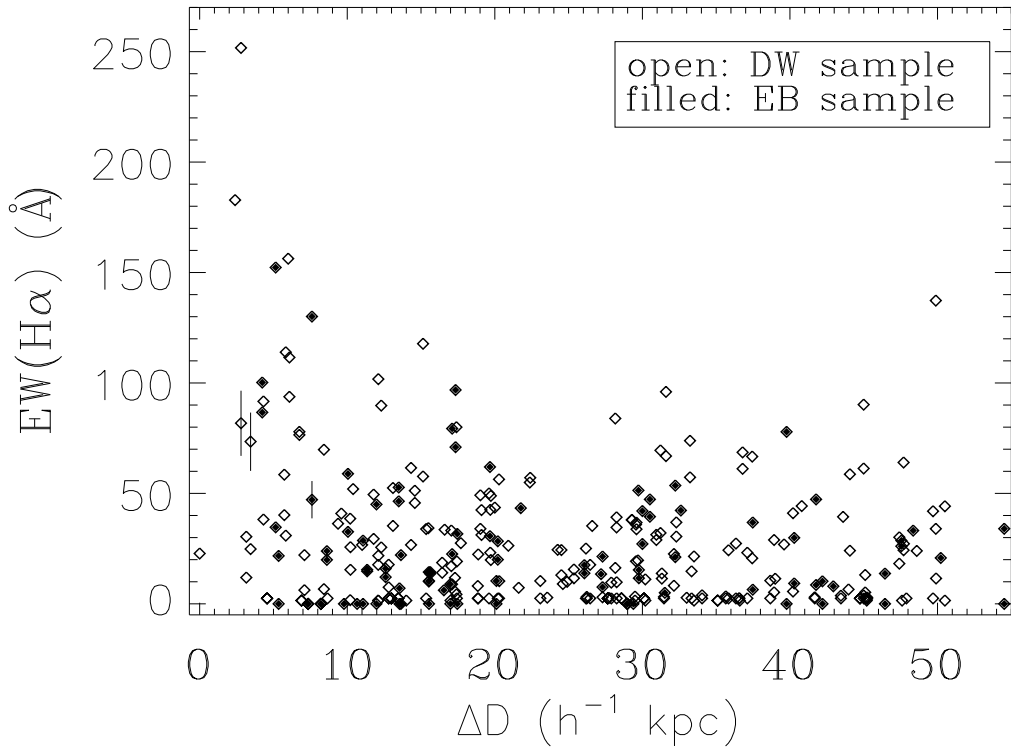


Fig. 8.— ΔD vs. $EW(H\alpha)$ for the 323 galaxies in the DW+EB sample. ΔD is the projected spatial separation to the nearest neighbor. Representative error bars show the measurement uncertainty of $\pm 18\%$ for $EW(H\alpha)$.

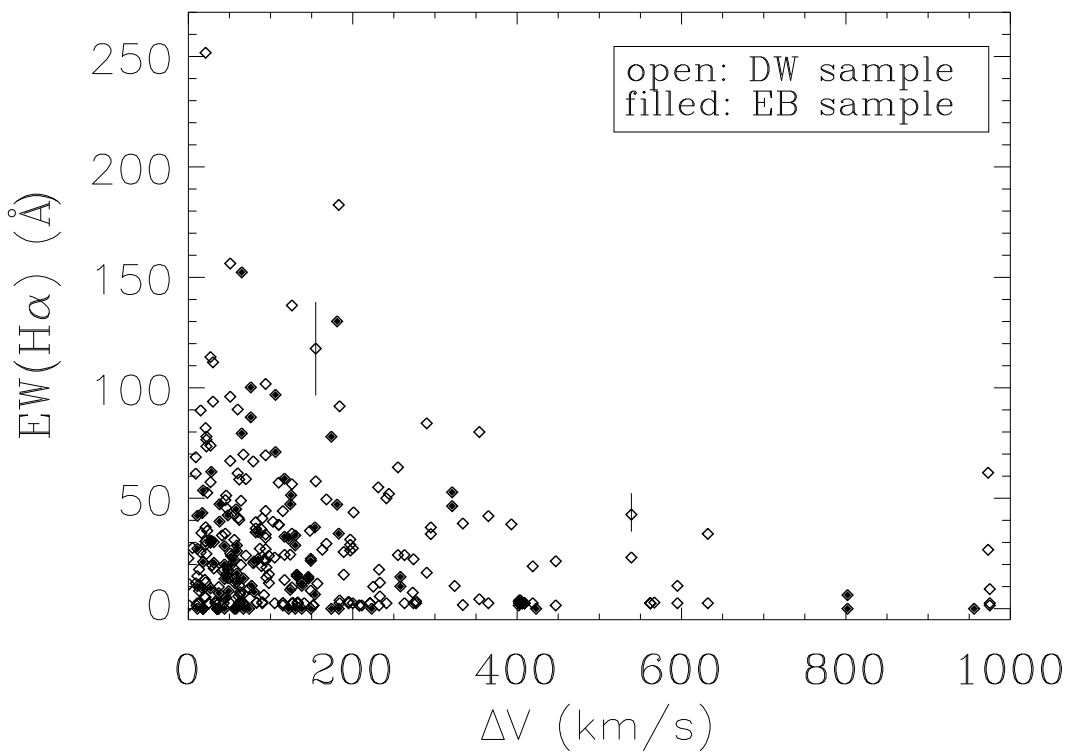


Fig. 9.— ΔV vs. $\text{EW}(\text{H}\alpha)$ for the 323 galaxies in the DW+EB sample. ΔV is the line-of-sight velocity separation to the nearest neighbor. Representative error bars are $\pm 18\%$ in $\text{EW}(\text{H}\alpha)$.

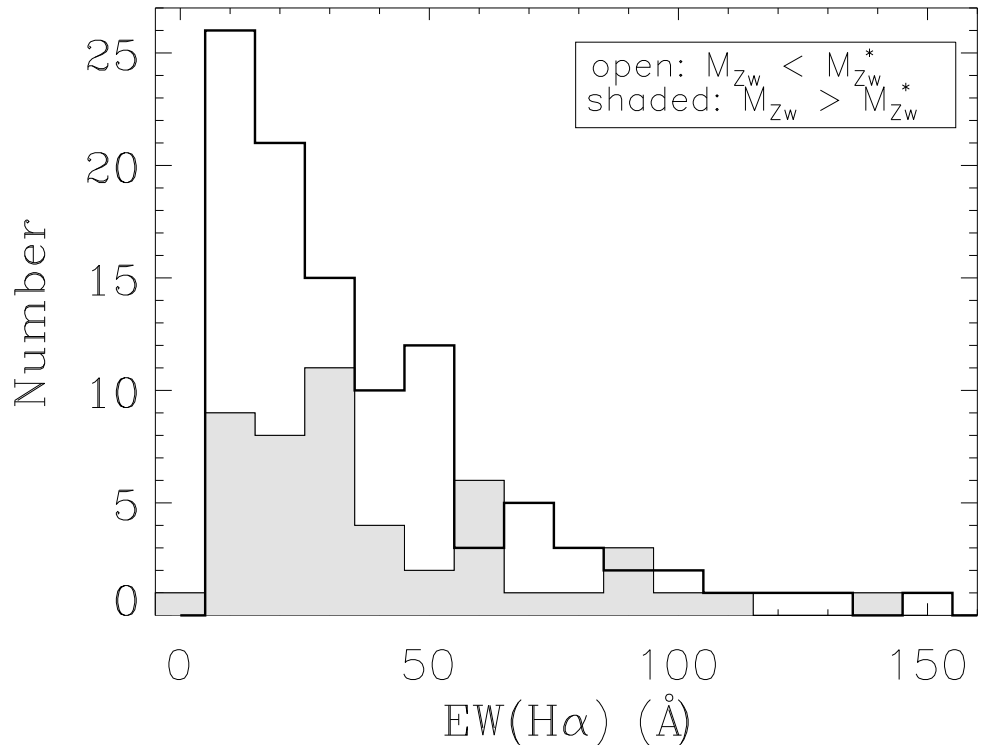


Fig. 10.— The distributions of $\text{EW}(\text{H}\alpha)$ for the $M_{Zw} > M_{Zw}^*$ and $M_{Zw} < M_{Zw}^*$ galaxies in the DW+EB sample. The 1σ fractional error in $\text{EW}(\text{H}\alpha)$ is 18%, and ± 0.41 mag for M_{Zw} . Not shown are the $\text{EW}(\text{H}\alpha) < 3.5$ Å (corrected for stellar absorption) galaxies, which make up 21% (13/62) of the $M_{Zw} > M_{Zw}^*$ sample and 27% (38/141) of the $M_{Zw} < M_{Zw}^*$ galaxies.

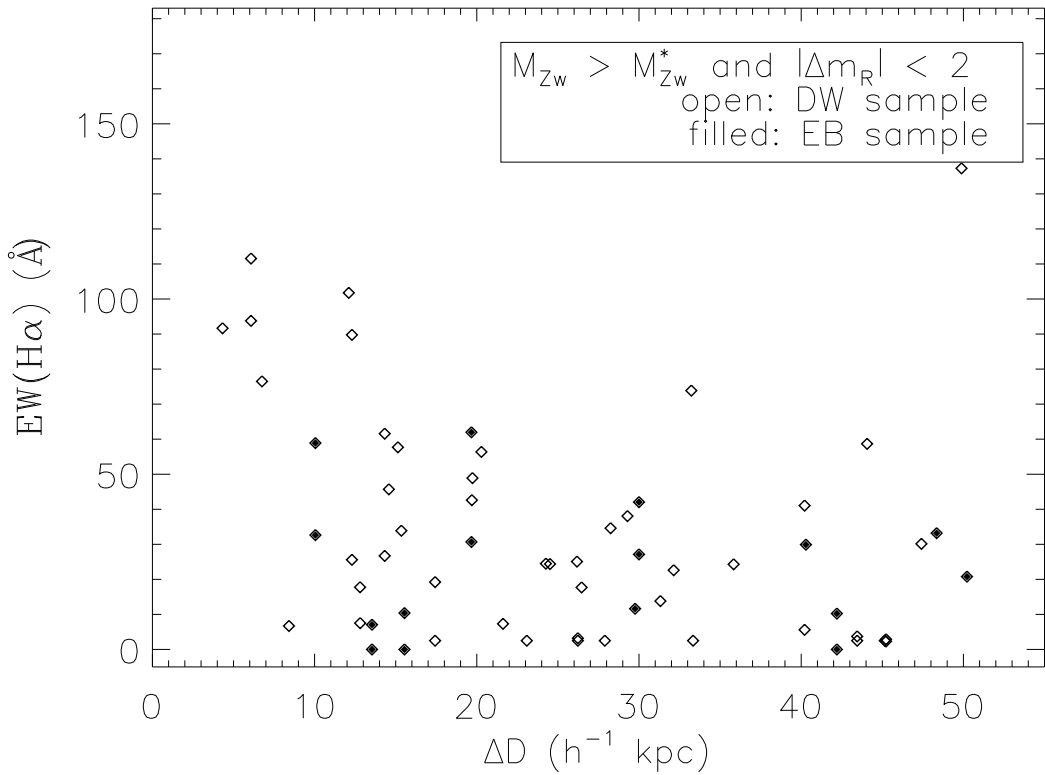


Fig. 11.— ΔD vs. EW(H α) for the galaxies in subsets of M_{Zw} . The 1σ fractional error is 18% in EW(H α), and ± 0.41 mag for M_{Zw} .

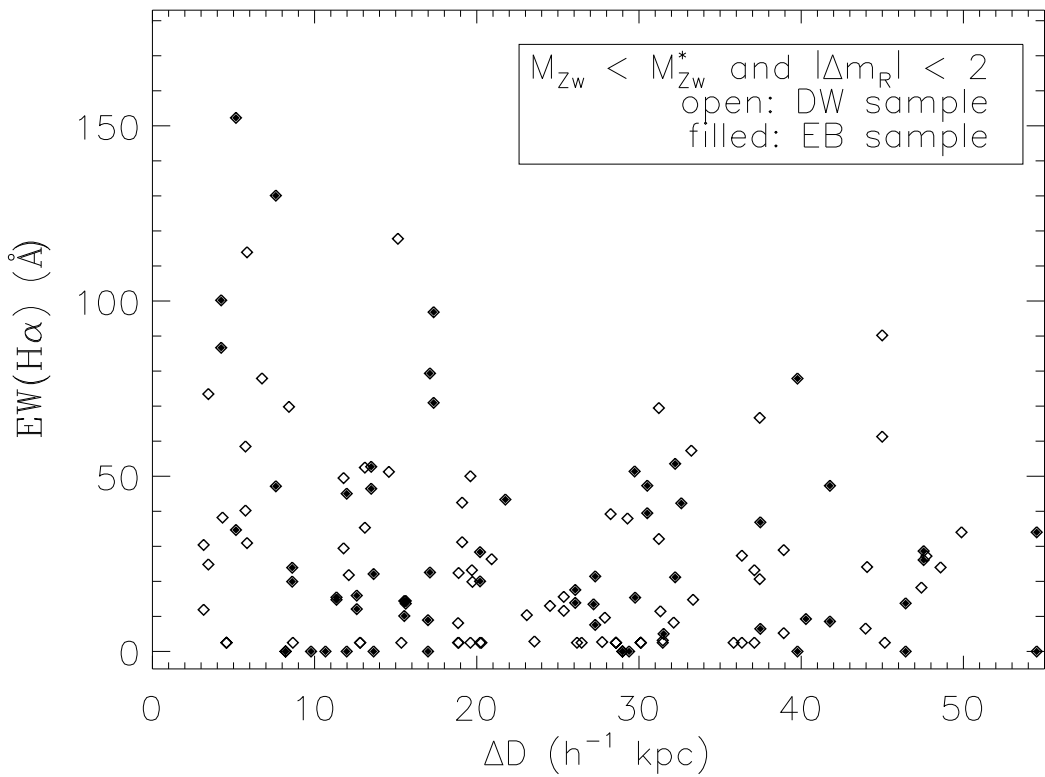


Fig. 12.— ΔD vs. $EW(H\alpha)$ for the galaxies in subsets of M_{Zw} . The 1σ fractional error is 18% in $EW(H\alpha)$, and ± 0.41 mag for M_{Zw} .

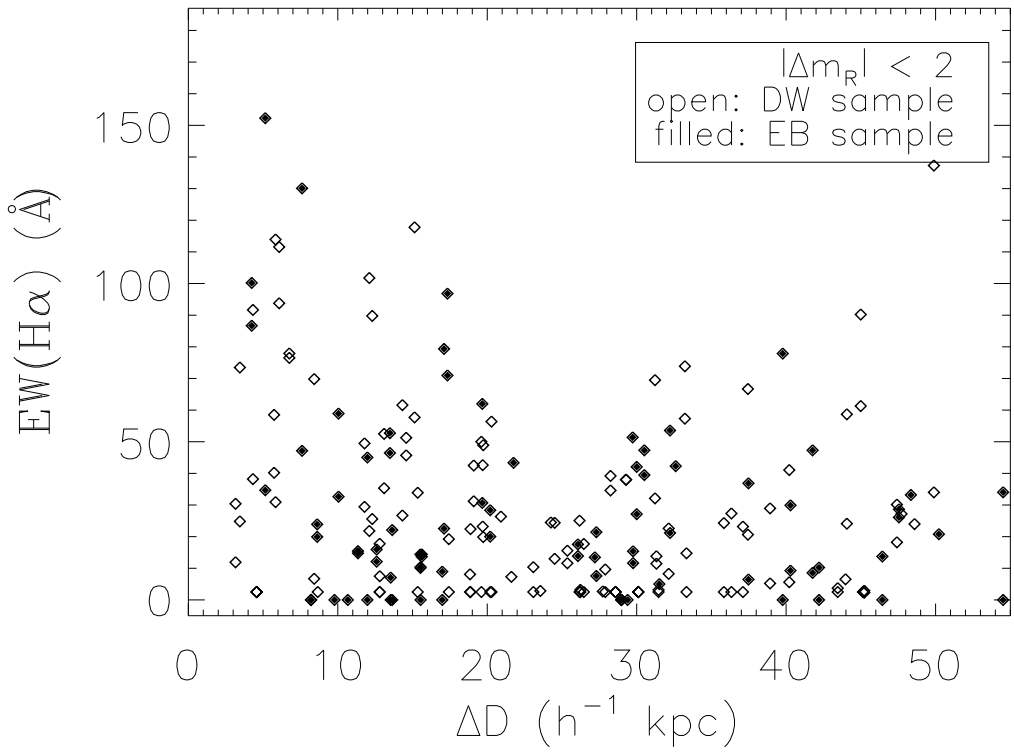


Fig. 13.— ΔD vs. $\text{EW}(\text{H}\alpha)$ for the galaxies in subsets of $|\Delta m_R|$. The 1σ fractional error is 18% for $\text{EW}(\text{H}\alpha)$, and 0.17 mag for $|\Delta m_R|$.

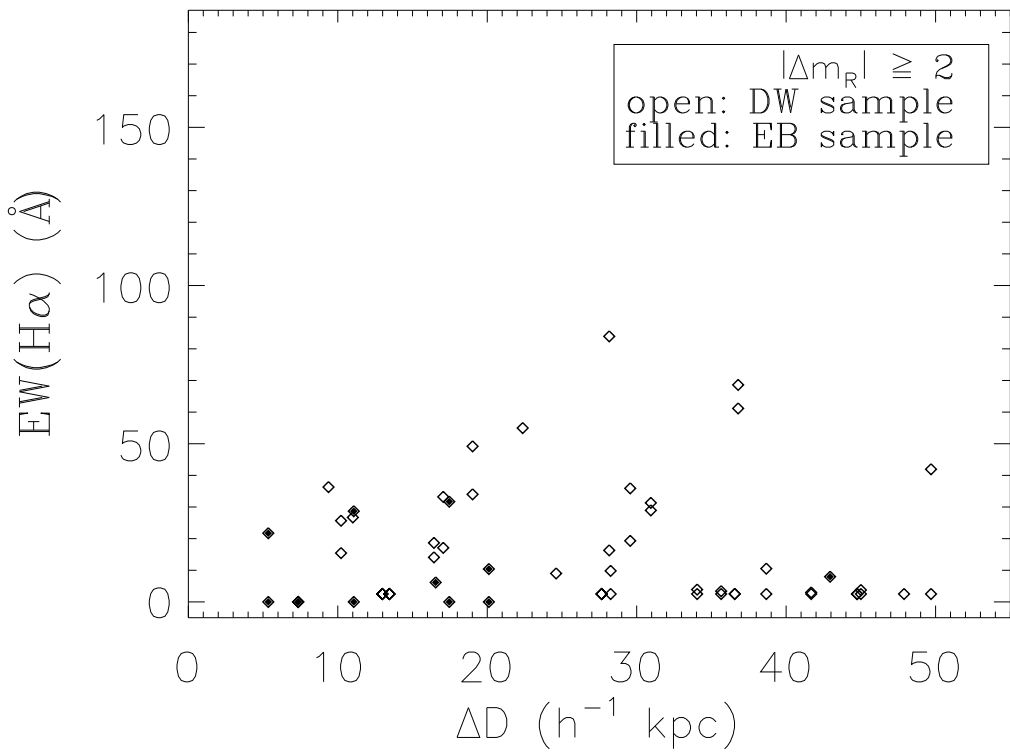


Fig. 14.— ΔD vs. $EW(H\alpha)$ for the galaxies in subsets of $|\Delta m_R|$. The 1σ fractional error is 18% for $EW(H\alpha)$, and 0.17 mag for $|\Delta m_R|$.

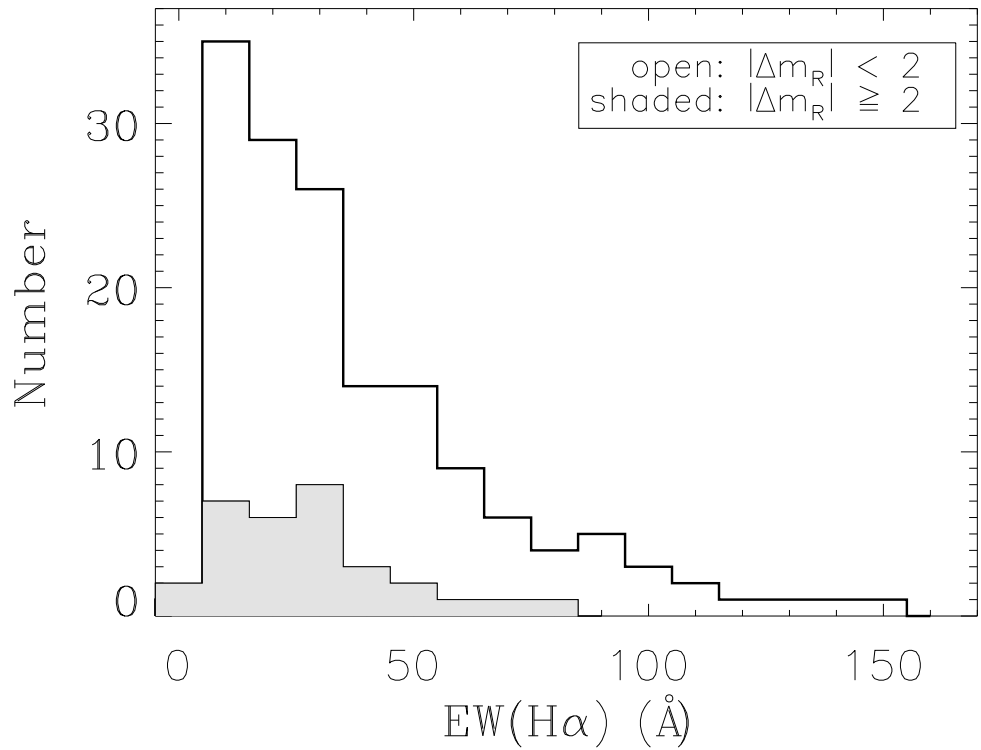


Fig. 15.— Distribution of EW(H α) for the $|\Delta m_R| < 2$ and $|\Delta m_R| \geq 2$ subsets. Note the absence of high EW(H α) for the $|\Delta m_R| \geq 2$ galaxies. Values of EW(H α) < 3.5 Å (corrected for Balmer absorption) are excluded from the plot. The EW(H α) < 3.5 Å make up 25% (51/203) of the $|\Delta m_R| < 2$ sample and 44% (24/55) of the $|\Delta m_R| \geq 2$ sample.

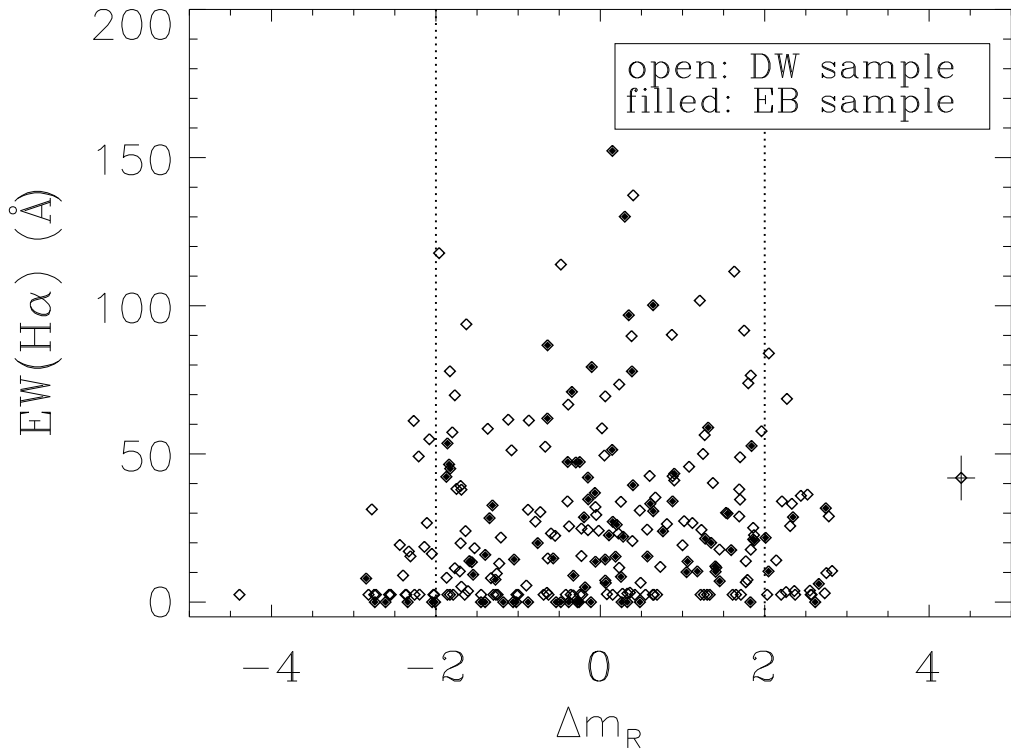


Fig. 16.— Δm_R vs. $\text{EW}(\text{H}\alpha)$ for the DW+EB sample. The brighter of the pair has $\Delta m_R < 0$, and the fainter of the pair has $\Delta m_R > 0$. Representative error bars of ± 0.17 mag in Δm_R and $\pm 18\%$ in $\text{EW}(\text{H}\alpha)$ are shown on the right most point.

Table 1. Galaxy data for members of pairs.*

ID	RA (J2000) h m s	Dec (J2000) ° ' "	cz ^a (km s ⁻¹)	EW(H α) ^b (Å)	Δm_R ^c	Type ^d
000348+17090_a	0 6 21.74	17 26 15.49	5770 ± 2	49	-0.3	gal
000348+17090_b	0 6 21.44	17 25 47.43	5589 ± 1	132	0.3	gal
081648+22120_a	8 19 48.49	22 1 57.68	3476 ± 9	2	-2.7	gal
081648+22120_b	8 19 41.34	22 2 30.30	3354 ± 4	33	2.7	gal
115454+32360_a	11 57 31.62	32 20 27.78	3259 ± 6	154	0.1	gal
115454+32360_b	11 57 43.95	32 17 39.62	3324 ± 9	81	-0.1	gal
120306+09160_a	12 5 36.29	8 59 15.90	6309 ± 9	23	1.3	gal
120306+09160_b	12 5 42.43	8 59 22.53	6230 ± 11	9	-1.3	gal
134412+44050_a	13 46 23.68	43 52 18.60	2490 ± 15	2	-2.3	gal
134412+44050_b	13 46 18.53	43 51 3.70	2360 ± 3	30	2.3	gal

*Full table appears in electronic edition.

^aError measurement is based on the derived r value (Tonry & Davis 1979) and the FWHM of the correlation peak used to obtain cz . See §3.2 in Kurtz & Mink (1998) for a detailed description of the error measurement.

^bEW(H α) is corrected for Balmer absorption. Error in EW(H α) is ±18%, described in §3.2.

^c $\Delta m_R < 0$ for the brighter of the pair and $\Delta m_R > 0$ for the fainter.

^dObject type: galaxy (gal), intermediate (int), or AGN.

Table 2. Galaxy data for non-member galaxies.*

ID	RA (J2000)	Dec (J2000)	cz ^a
			h m s
001412+06470_b	0 16 38.79	7 6 55.33	11851 ± 20
002018+06330_b	0 22 53.52	6 49 38.22	15100 ± 20
003648+36050_b	0 39 33.52	36 23 33.42	16120 ± 16
004154+16320_c	0 44 33.32	16 50 12.59	23843 ± 17
004212+04530_b	0 44 57.93	5 8 44.96	38646 ± 31
004336+19130_b	0 46 8.60	19 31 16.70	29611 ± 28
004336+19130_e	0 46 12.54	19 33 20.50	28511 ± 30
004736-02120_b	0 50 5.55	-1 55 59.47	24282 ± 18
005706+17450_b	0 59 40.29	17 58 25.31	26257 ± 17
010218+04300_b	1 4 44.73	4 47 27.14	13754 ± 16

*Full table appears in electronic edition.

^aError measurement is based on the derived r value (Tonry & Davis 1979) and the FWHM of the correlation peak used to obtain cz . See §3.2 in Kurtz & Mink (1998) for a detailed description of the error measurement.

Table 3. Absolute photometry for galaxies in DW sample.

ID	RA (J2000)	Dec (J2000)	M_R ^a	M_B ^a	Obs. Date
			h m s	° ' "	
142812+00280_a	14 30 45.92	0 14 52.39	-23.59	-21.51	2003 Jun 01
142812+00280_b	14 30 43.03	0 15 11.12	-23.20	-21.15	2003 Jun 01
143412+02360_a	14 36 41.93	2 23 9.61	-21.34	-19.34	2003 Jun 01
143412+02360_b	14 36 41.43	2 22 26.25	-20.26	-18.22	2003 Jun 01
150200+42180_a	15 3 50.43	42 6 56.10	-22.47	-20.00	2003 Jun 01
150200+42180_b	15 3 39.71	42 7 34.45	-20.60	-18.28	2003 Jun 01

^aError in M_B and M_R is 0.12 mag.

Table 4. Comparison of EW(H α) in different samples.

Sample	> 10 Å	> 40 Å	> 70 Å	Num. Gal.
DW	59%	23%	9%	231
15R-North ^a	25%	4%	0.2%	1675
EB	66%	23%	9%	92
UZC ^b	36%	6%	2%	12562

^aGalaxies selected to match redshift range and apparent magnitude range of DW sample: $2300 < cz < 16500 \text{ km s}^{-1}$, and $m_R < 17$. Galaxies with AGN-like spectra are excluded.

^bGalaxies selected with $2300 < cz < 16500 \text{ km s}^{-1}$, and $m_{ZW} < 18$.